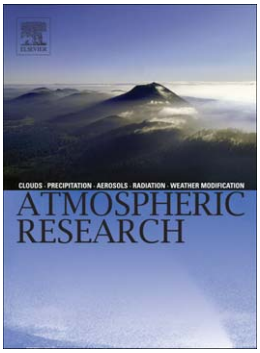

Implementation of non-local boundary layer schemes in the regional atmospheric modelling system and its impact on simulated mesoscale circulations

I. Gómez, R.J. Ronda, V. Caselles, M.J. Estrela

PII: S0169-8095(16)30118-1
DOI: doi: 10.1016/j.atmosres.2016.04.020
Reference: ATMOS 3689

To appear in: *Atmospheric Research*

Received date: 26 February 2016
Revised date: 20 April 2016
Accepted date: 28 April 2016

Please cite this article as: Gómez, I., Ronda, R.J., Caselles, V., Estrela, M.J., Implementation of non-local boundary layer schemes in the regional atmospheric modelling system and its impact on simulated mesoscale circulations, *Atmospheric Research* (2016), doi: 10.1016/j.atmosres.2016.04.020

Implementation of Non-local Boundary Layer schemes in the Regional Atmospheric Modeling System and its impact on simulated mesoscale circulations

I. GÓMEZ[a,b], R. J. RONDA[c], V. CASELLES[a], M. J. ESTRELA[d]

[a] *Earth Physics and Thermodynamics Department, Faculty of Physics, University of Valencia, Doctor Moliner, 50, 46100 Burjassot, Valencia, Spain.*

[b] *Environment and Earth Sciences Department, Faculty of Sciences, University of Alicante, Section 99, E-03080, Alicante, Spain.*

[c] *Meteorology and Air Quality Group, Wageningen University and Research Center, Wageningen, Netherlands.*

[d] *Geography Department, Faculty of Geography and History, University of Valencia, Avda. Blasco Ibáñez, 28, 46010 Valencia, Spain.*

Correspondence to: Igor Gómez

E-mail: Igor.Gomez@uv.es

ABSTRACT

This paper proposes the implementation of different non-local Planetary Boundary Layer schemes within the Regional Atmospheric Modeling System (RAMS) model. The two selected PBL parameterizations are the Medium-Range Forecast (MRF) PBL and its updated version, known as the Yonsei University (YSU) PBL. YSU is a first-order scheme that uses non-local eddy diffusivity coefficients to compute turbulent fluxes. It is based on the MRF, and improves it with an explicit treatment of the entrainment. With the aim of evaluating the RAMS results for these PBL parameterizations, a series of numerical simulations have been performed and contrasted with the results obtained using the Mellor and Yamada (MY) scheme, also widely used, and the standard PBL scheme in the RAMS model. The numerical study carried out here is focused on mesoscale circulations events during the summer, as these meteorological situations dominate this season of the year in the Western Mediterranean coast. In addition, the sensitivity of these PBL parameterizations to the initial soil moisture content is also evaluated. The results show a warmer and moister PBL for the YSU scheme compared to both MRF and MY. The model presents as well a tendency to overestimate the observed temperature and to underestimate the observed humidity, considering all PBL schemes and a low initial soil moisture content. In addition, the bias between the model and the observations is significantly reduced moistening the initial soil moisture of the corresponding run. Thus, varying this parameter has a positive effect and improves the simulated results in relation to the observations. However, there is still a significant overestimation of the wind speed over flatter terrain, independently of the PBL scheme and the initial soil moisture used, even though a different degree of accuracy is reproduced by RAMS taking into account the different sensitivity tests.

Keywords: RAMS model, boundary layer, mesoscale modelling, PBL parameterization, Non-local schemes, numerical weather prediction/forecasting

1. Introduction

Parametrization schemes describe the contribution of unresolved atmospheric phenomena in terms of variables resolved at the model's discrete grid. An important parameterization is the Planetary Boundary Layer (PBL) scheme, which accounts for the vertical transport in the turbulent PBL, and where the air layers are directly affected by the Earth's surface. Vertical transport of heat, moisture, momentum and other physical properties of the lower troposphere are driven by PBL processes (Hu et al., 2010), and low level clouds (Hariprasad et al., 2014). Therefore, a correct parametrization of the processes in the PBL is essential to achieve realistic simulations (Steeneveld et al., 2008; García-Díez et al., 2013).

PBL parametrizations can be classified depending on how they approach the turbulence closure problem. Local closure schemes use solely variables and parameters that are defined at each model level or its neighbours (e.g local gradients). In contrast, non-local closure schemes use in addition to local parameters, other variables that depend on part of the whole vertical profile of heat, moisture and momentum within the PBL, while in addition local eddy-diffusivity coefficients can be functions of relationships between separated levels (e.g. diffusion coefficients dependent on the PBL thickness). This is often summarized by referring to them as local and non-local schemes (García-Díez et al., 2013). Local schemes often use a Turbulent Kinetic Energy (TKE) closure, based on Mellor and Yamada (1982) (MY hereafter), and have become popular, since they can represent the entrainment with the diffusion of the TKE and the so-called counter-gradient terms, that allow diffusion against the local gradients (Deardorff, 1966). The MY scheme has been widely used within the framework of the Regional Atmospheric Modeling System (RAMS) (Cotton et al., 2003; Pielke, 2013). Additionally, several Mellor-Yamada-based PBL schemes have been developed within

other mesoscale numerical weather prediction systems, such as the Weather Research and Forecasting (WRF) model (Skamarock et al., 2008): the Mellor–Yamada–Janjic (MYJ) TKE closure (Janjic, 1994) and the Mellor–Yamada–Nakanishi–Niino level 2.5 (MYNN) local closure (Nakanishi and Niino, 2004).

The main aim of the present study is to implement different non-local Boundary Layer schemes within the latest version of the RAMS model (Version 6.0) to be used as an alternative to the MY scheme. Particularly, we have chosen the Medium-Range Forecast (MRF) PBL (Troen and Mahrt, 1986; Hong and Pan, 1996) and its updated version known as the Yonsei University (YSU) PBL (Hong et al., 2006). In this regard, the YSU scheme is a first order, modified MRF scheme. Since the MRF scheme lacks an explicit entrainment formulation at the PBL top, and also because momentum transfer is only local and downgradient, Hong et al. (2006) extended the MRF scheme with an entrainment flux at the top of the PBL (Steeneveld et al., 2011). The entrainment is made proportional to the surface buoyancy flux while the PBL top is defined as the layer where the bulk Richardson becomes lower than zero (Hong, 2010). Additionally, in contrast to the MRF scheme, YSU uses a Prandtl number formulation that allows the Pr to be variable in the vertical profile. Finally, the improvement of the K-profile model included in Noh et al. (2003) and the new stable boundary-layer mixing scheme proposed by Hong (2010) are also considered here. In the next section, the MRF and the YSU schemes are introduced in more detail.

With the continuous developments in models and improvements in PBL physics, several intercomparison studies have been made to study the suitability and application of specific schemes over different regions and using different Mesoscale Meteorological Models (see e.g. Cuxart et al., 2006; Steeneveld et al., 2008; Hu et al., 2010; Shin and Hong, 2011; Steeneveld et al., 2011; García-Díez et al., 2013; Hariprasad et al., 2014;

Kleczek et al., 2014). For example, using the WRF model framework, Steeneveld et al. (2011) found that the largest differences between the MRF and the YSU schemes occur at night during strong winds. Additionally, Hu et al. (2010) compared the YSU scheme with the MYJ scheme over Texas using a series of simulations spanning three months during summer 2005 and using the WRF as a host model as well. They found that YSU leads to predictions of higher temperature and lower moisture, with smaller biases than MYJ in the lower atmosphere both at day and night time. In the former case because of its stronger vertical mixing, while in the latter because of its enhanced mixing during nighttime. Furthermore, previous works show that, in general, local schemes tend to produce unrealistically shallow and moist boundary layers (e.g. Hong et al. 2006). This is related to their inability to directly represent large-scale turbulence and the underestimation of entrainment. Other works show, however, that non-local schemes are not always more skilful (Deng and Stauffer, 2006), and that they can produce too deep boundary layers in windy conditions (Braun and Tao, 2000; Steeneveld et al., 2011).

In addition, other intercomparison studies have been applied specifically to mesoscale circulations in coastal areas (see e.g. Srinivas et al., 2007; Zhong et al., 2007; Miao et al., 2008; Miao et al., 2009; Challa et al., 2009). For instance, Challa et al. (2009) used the MYJ and the YSU scheme in the Mississippi Gulf coast implemented within the WRF environment. This study showed that the diurnal variation in the surface wind direction is better represented with MYJ scheme. In addition, the simulated sea breeze front was more intense in the case with YSU PBL, which produced higher surface convergence, upward divergence and vertical motion than the MYJ scheme.

Finally, as compared to MYJ, YSU scheme tended to produce more realistic mixing heights both at the coast and inland. Day time mixed layer produced by the MYJ

scheme is deeper near the coast and shallow far inland than that simulated using YSU scheme. In another recent study a comparison between the MYJ, the MYNN local closure and the YSU scheme is performed using the WRF model as well (Hariprasad et al., 2014). In this case, MYJ and MYNN simulated humidity reasonably well while YSU produced large dry bias in the night time. MYJ considerably overestimated the winds while YSU simulated moderately stronger winds relative to observations. The results obtained by Hariprasad et al. (2014) corroborate the findings from earlier intercomparison studies by Hu et al. (2010), Shin and Hong (2011) and Steeneveld et al. (2008) using the WRF model.

Thus, additionally to the implementation of the MRF and the YSU parameterizations within the RAMS framework, the second aim of the current paper is based on evaluating the effect and influence of both PBL schemes in the model results when compared to the MY scheme. In this regard, we have performed an intercomparison study focused on summer mesoscale circulations over a Western Mediterranean area. The main reason to select these sort of atmospheric conditions is because they prevail against other meteorological frameworks during the summer months in this region (Azorin-Molina et al., 2011; Azorin-Molina et al., 2014; Gómez et al., 2014a,b; Gómez et al., 2015a,b). In this regard, it is well known that under weak synoptic forcing, local scale circulations can prevail in coastal areas (Pielke, 2013). The land-sea temperature contrast is also significantly higher during summer and causes sea breeze induced convection and local thunderstorms (Pielke, 2013; Azorin et al., 2014). Thus, we have selected two mesoscale circulations from the 2011 summer season: the 25-26 June and the 11-12 August periods. Considering these two distinct events, we would like to focus on one event at the beginning of the summer season and another one into this season, so as to test whether significant differences on mesoscale circulations

arises within the summer and considering the MY in comparison with the MRF and the YSU schemes. The period 25-26 June was selected considering a situation where clear skies dominates the atmospheric conditions while the 11-12 August period was selected to include conditions prone to summer storms (Azorin et al., 2014).

The paper is organised as follows. Section 2 contains an overview of the MRF and YSU PBL parameterizations. A description of the study area as well as the model configuration and the observational datasets is introduced in section 3. In addition, a detailed description of the experimental design is also provided in this section. In section 4, we introduce the synoptic framework for the simulated periods and the model results. Finally, section 5 is devoted to the discussion and the concluding remarks.

2. Implementation of the non-local PBL packages

In order to understand the model development and results, a brief description of the formulation for both the MRF and the YSU parameterizations is included in this section. A complete description of the MRF scheme is given in Hong and Pan (1996). According to Troen and Mahrt (1986), the turbulent diffusion equation for prognostic variables (C; u, v, θ, q) can be expressed by

$$\frac{\partial C}{\partial t} = \frac{\partial}{\partial z}\left[K_c\left(\frac{\partial C}{\partial z} - \gamma_c\right)\right] \tag{1}$$

where K_c is the eddy diffusion coefficient and γ_c is a correction to the local gradient that incorporates the contribution of the large scale eddies to the total flux (Hong and Pan, 1996). Equation (1) corresponds to the MRF scheme, where the counter gradient correction applies to θ and q within the mixed boundary layer. As we will see here, the non-local diffusion approach is adapted for mixed-layer diffusion, while above this layer, the local diffusion approach is applied to account for free atmosphere diffusion.

The counter gradient term within the mixed boundary layer is given by

$$\gamma_c = b\frac{\left(\overline{w}'c'\right)}{w_s} \tag{2}$$

where $\left(\overline{w}'c'\right)$ is the corresponding surface flux for θ and q, while b is a coefficient of proportionality (=7.8). In addition, the momentum diffusivity coefficient below the PBL is prescribed as

$$K_m = kw_s z\left(1-\frac{z}{h}\right)^2 \tag{3}$$

where k is the Von Karman constant (=0.4), z is the height from the surface, and h is the height of the PBL. The eddy diffusivity K_h in (1) is computed from K_m by using the Prandtl number Pr, which is determined by the stability at the top of the surface layer, as $K_h = Pr^{-1} K_m$. In the original formulation of the MRF scheme by Hong and Pan (1996), the Prandtl number is given by

$$Pr = \left(\frac{\varphi_h}{\varphi_m} + bk\frac{0.1h}{h}\right) \tag{4}$$

where Pr is a constant within whole mixed boundary layer.

The velocity scale w_s in (2) is represented by the value scaled at the top of the surface layer, w_{s0} such as

$$w_s = u\ \Phi_m^{-1} \tag{5}$$

where u is the surface frictional velocity scale and Φ_m^{-1} is the wind profile function evaluated at the top of the surface layer.

The value of Φ_m is obtained by satisfying the compatibility with the surface boundary similarity. The profile functions for momentum and heat, Φ_m and Φ_h, are given respectively by

$$\Phi_m = \Phi_h = \left(1+5\frac{0.1h}{L}\right) \tag{6}$$

for stable conditions, and

$$\Phi_m = \left(1 - 16\frac{0.1h}{L}\right)^{-1/4} \quad \text{, for u and v} \tag{7}$$

$$\Phi_h = \left(1 - 16\frac{0.1h}{L}\right)^{-1/2} \quad \text{, for } \theta \text{ and q} \tag{8}$$

for unstable conditions, where L is the Monin-Obukhov length scale.

Additionally, the boundary layer height is given by

$$h = Rib_{cr}\frac{\theta_{va}|U(h)|^2}{g\left(\theta_v(h) - \theta_s\right)} \tag{9}$$

where Rib_{cr} is the critical bulk Richardson number, U(h) is the horizontal wind speed at h, and θ_{va} is the virtual potential temperature at the lowest model level, $\theta_v(h)$ is the virtual potential temperature at h, θ_s is the appropriate temperature near the surface. Numerically, the boundary layer height, h, is obtained iteratively (see Hong and Pan, 1996; Noh et al., 2003; Hong et al., 2006; Hong, 2010).

Above the mixed layer (free atmosphere), the local diffusion scheme proposed by Louis (1979) is used. In this scheme, the vertical diffusivity coefficients for momentum(m; u, v) and scalars (h; θ , q), following Louis (1979) above h, are represented by

$$K_{m,h} = l^2 f_{m,t}(Ri_g)\left(\frac{\partial U}{\partial z}\right) \tag{10}$$

in terms of the mixing length l, the stability functions $f_{m,t}$ (Ri_g), and the vertical wind shear, $|\partial U/\partial z|$. The stability functions $f_{m,t}$ are represented in terms of the local gradient Richardson number Ri_g.

The mixing length-scale l is given by

$$\frac{1}{l} = \frac{1}{kz} + \frac{1}{\lambda_0} \tag{11}$$

where z is the height from the surface. Here λ_0 is the asymptotic length-scale (=30 m).

Although the original Rib_{cr} was set to 0.5, in the current study we have used a value of 0.25, consistent with those used in different studies within the Iberian Peninsula (Borge et al., 2008; Hernández-Ceballos et al., 2013). Additionally, we must remark here that the stability functions $f_{m,t}$ are represented in terms of the local gradient Richardson number Rig, considering that Rig is modified for reduced stability within cloudy air. Moreover, the stability functions $f_{m,t}$ (Rig) differ for stable and unstable regimes. In this case, we have adopted the stability formulas used by Hong et al. (2006) instead of the original ones used in Hong et al. (1996). This modification of the MRF model is in accordance with the modifications implemented in this PBL scheme within other mesoscale models, such as the WRF Model (Hong et al., 2006).

These last variations proposed by Hong et al. (2006) in relation with the original MRF scheme developed by Hong et al. (1996) are preserved in the YSU scheme as well. This parameterization is a modified K-theory, with an additional countergradient term that incorporates the contribution of large-scale eddies to the total flux. The turbulence diffusion equations for prognostic variables C (zonal wind u, meridional wind v, potential temperature θ , specific humidity for water vapour q, cloud water mixing ratio q_c, cloud ice mixing ratio q i) can be expressed by (Hong, 2010)

$$\frac{\partial C}{\partial t}=\frac{\partial}{\partial z}\left[K_c\left(\frac{\partial C}{\partial z}-\gamma_c\right)-\left(\overline{w}'c'\right)_h\left(\frac{z}{h}\right)^3\right] \tag{12}$$

, $\left(\overline{w}'c'\right)_h$ is the flux at the inversion layer. The PBL height h is defined as the level in which minimum flux exists at the inversion level. A complete description of the YSU scheme is given in Hong et al. (2006). A theoretical development of the explicit entrainment processes algorithm in the YSU scheme is given in Noh et al. (2003).

In the YSU model, the mixed-layer velocity-scale is represented as

$w_{s0} = (u^{3} + 8kw_{b}^{3}z/h)^{1/3}$

(13)

where u is the surface frictional velocity-scale, and the convective velocity-scale for moist air is

$w_{b} = [(g/\theta_{va})(w'\theta_{v}')_{0} h)]^{1/3}$ (14)

In this case, the counter gradient term for θ and momentum changed equation (2) to the next one

$$\gamma_c = b\frac{(\overline{w}'c')_0}{w_{s0}} \quad (15)$$

where $(\overline{w}'c')_0$ is the corresponding surface flux for θ , u, and v. The mixed-layer w_{s0} in (15) is defined as the velocity at z = 0.5 h in (13). The eddy diffusivity K_h for temperature and moisture is computed from K_m in (3) by using the relationship of the Prandtl number. As a difference with the MRF model, the YSU scheme does not apply the counter gradient term to q, but to u and v. Additionally, the MRF assumes that the Prandtl number remains invariant with height. Nevertheless, the stability of the convective boundary layer itself changes from unstable near the surface layer to stable at the upper boundary. Accordingly, the Prandtl number is also expected to vary within the PBL (Noh et al., 2003). Thus, the profile of the Prandtl number is proposed to vary as

$P_r = 1 + (P_{r0} - 1)\exp[-\alpha(z - \varepsilon h)^2 / h^2]$ (16)

where P_{r0} is the Prandtl number at the top of the surface layer given by (4) and α is an empirical constant (=0.3).

The flux at the inversion layer for scalars θ and q, and vector quantities u and v, is proportional to the jump of each variable at the inversion layer, such as

$$(\overline{w}'c')_h = w_e \Delta c_h \quad (17)$$

where w_e is the entrainment rate at the inversion layer (Hong et al., 2006). In addition, Noh et al. (2003) considers the entrainment flux above h so as to express the penetration of entrainment flux above h irrespective of local stability. Here, we consider both effects within the entrainment zone and the local K approach above. More details about the free atmosphere diffusion and the parameterization of the entrainment zone can be consulted in Hong et al. (2006).

Finally, a revised stable boundary-layer (SBL) parameterization in included according to Hong (2010), where the surface bulk Ri method with a Rossby-number-dependent critical value, $Ri_{b,cr}$, is used, expressed by

$$Ri_{b,cr} = 0.16(10^{-7}\,Ro)^{-0.18} \quad (18)$$

where Ro is the surface Rossby number, which is given by

$$Ro = U_{10}/(f_0 z_0) \quad (19)$$

where U_{10} is the wind speed at 10 m from the surface, f_0 ($=10^{-4}$ m) the Coriolis parameter, and z_0 the surface roughness length.

3. Numerical simulations and methodology

Both the MRF and the YSU schemes with the changes described above have been implemented in the RAMS model (Cotton et al., 2003; Pielke, 2013), using version 6.0. In order to test these parameterizations, several numerical simulations have been performed with this model focused in the Valencia Region (Western Mediterranean Basin) (Fig. 1). RAMS utilised and operated as a non-hydrostatic, compressible, primitive equation model with a σ_z terrain-following vertical coordinate system with polar stereographic coordinates. In addition, RAMS 6.0 is coupled to a Land-Ecosystem Atmosphere Feedback Model (LEAF-3) that represents the energy and moisture budgets at the surface and their interactions with the atmosphere (Walko et al. 2000). It

incorporates the interactions between soil and vegetation, and each on the atmosphere at a subgrid scale; see Walko et al. (2000) for detailed model descriptions.

RAMS was initialized using the National Centre for Environmental Prediction (NCEP) Global Final Analysis (FNL) at 6 h intervals and 1 x 1 degree resolution globally. In addition, a Four-Dimensional Data Assimilation (FDDA) technique was applied to define the forcing at the lateral boundaries of the outermost five grid cells of the largest domain. Three nested grids were used (Fig. 1) with horizontal resolution of 48 km, 12 km and 3 km. In the vertical, a total of 45 levels were selected following a stretched scheme, with a 30-m spacing near the surface increasing gradually up to 1,000 m near the model top at about 16,000 m and with 15 levels in the lower 1,000 m.

All simulations used the Chen-Cotton scheme for longwave and shortwave radiation (Chen and Cotton 1983), and the Kuo-modified scheme (Molinari et al., 1985) for convection on the outer grid (Gómez et al., 2014a,b; Gómez et al., 2015a,b).

Two different mesoscale circulation frameworks were selected, corresponding to the periods 25-26 June and 11-12 August 2011. Each simulation was performed for 60 h, with a temporal resolution of 1 h, starting at 12 UTC 24 June 2011 for the June period and at 12 UTC 10 August 2011 for the August framework. The first 12 h are treated as a spin-up period to avoid possibles problems related to this initialization. Consequently, the analysis will be fulfilled using the remaining 48-h. For each of these simulation cycles, different runs has been operated using the MY, MRF and YSU schemes. Additionally, considering that we focus the current work on mesoscale circulations, the response of these parameterizations to the initial soil moisture (SM) content has been evaluated as well. The role of the soil moisture initialization on modelling results has also been evaluated in other studies (see e.g. Angevine et al., 2014; Daniels et al., 2015; Gómez et al., 2015b; Kalverla et al., 2016). In this regard, a set of sensitivity

simulations have been performed for each of the PBL parameterizations. Using MY, MRF and YSU schemes to investigate the influence of initial SM content is a commonly used configuration in modelling studies (see e. g. Tolk et al., 2009; Gómez et al., 2015b; Kalverla et al., 2016). In these experiments, two different SM values are used to initialize this parameter at a constant value for all land grid points and all soil levels: a low value of 0.2 m^3 m^{-3}, representing the moisture content of the soil as a fraction of the total water capacity that the soil can hold, and a high value of 0.4 m^3 m^{-3}, doubling the original. The two SM values used in the current study corresponds to the extremes previously applied by Gómez et al. (2015b). As a result, a total of six simulations were carried out for each selected period: MY20 (MY scheme with the lowest value of SM), MY40 (MY scheme with the highest value of SM), MRF20 (MRF scheme with the lowest value of SM), MRF40 (MRF scheme with the highest value of SM), YSU20 (YSU scheme with the lowest value of SM) and YSU40 (YSU scheme with the highest value of SM).

4. Results

4.1. Cases description

In this section, a brief description of the two selected cases is included. First of all, we must highlight that in both atmospheric situations, the Iberian Thermal Low (ITL; Millán et al., 1997; Millán et al., 2000) is developed (Fig. 2). For the 25-26 June 2011 period (Fig. 2a,b), this low pressure influences the west part of the Iberian Peninsula. On the other hand, a high pressure centre affects the north of Spain the 25 June, that is displaced to the centre of Europe the 26 and affects mainly the centre and east part of Spain extending to the Mediterranean and Europe. In contrast, the west of the Iberian Peninsula is under the influence of relative low pressures associated with the low pressure over the British Islands. For this simulation period, the 500 hPa data shows that

fair weather conditions are established over the Iberian Peninsula, influenced by high pressures and the -10 ºC isotherm positioned over this area. This fair weather is also supported by satellite images (not shown). Under this atmospheric framework, mesoscale circulations are expected over eastern Spain.

The 11 August 2011, the Iberian Thermal Low is also developed affecting the west part of the Iberian Peninsula (Fig. 2c). This low pressure system is deepened the 12 August, greatly influencing the centre of the Iberian Peninsula (Fig. 2d). This synoptic configuration produces instability over this area, as shown in the significant cloudiness observed in the satellite images (not shown). Besides, the surface situation favours a south-westernly advection to the north-east coast of Spain, reaching the Iberian System (Teruel Province; Fig. 1), that in addition to the a low pressure located over the Western Mediterranean, and promoting a north-eastern wind flow, produces a located cloudy development and precipitation storms over the mentioned area the 12 August 2011. However, the remaining east part of Spain shows in general fair weather, and remains under the influence of mesoscale circulations.

4.2. Model comparison with surface weather stations

We focus the discussion on the time series from five stations (SAN, SEG, XAT, VIL and VQM), as shown in Fig. 1. As the onset of a sea breeze in the Valencia Region is establish between 8:00-10:00 UTC (Azorin et al., 2009), it is usually characterised by an increase in near-surface temperature at sunrise due to the diurnal heating (Fig. 3), as well as an increase in wind speed (Fig. 4) and a clear change in wind direction (Fig. 5). We can observe a strong diurnal oscillation, characterized by the daytime development of the sea-breeze advecting air from sea to land, followed by night time surface drainage winds oriented from land to sea. Thermal circulations develop during the day, stabilizing a flow pattern advecting air from sea to land (Fig. 5).

In terms of the 2-m temperature (Fig. 3), RAMS reproduces the general qualitative trends associated with the sea breeze. It is observed that SM20 produces warmer results when compared to SM40, for the three PBL schemes. In this regard, the tendency of RAMS for any of these PBL representations is to overestimate the maximum temperatures using SM20. It seems that MRF fits better the observations in general for nocturnal temperatures, while YSU tends to over-predict this magnitude. Thus, in general, there is a warm bias that persist throughout the day. Contrasting the different parameterizations, some differences appear between the simulated days. On the one hand, the YSU scheme is warmer than both MY and MRF in the August period for the whole day, while the response of these last two schemes is rather alike, independently of the SM value. On the other hand, although this result for the August period is also true for the June period using SM40, the maximum temperature forecast by MRF is colder than the one reproduced by both MY and YSU applying SM20, which remains rather similar for the June period. In terms of processes, the diurnal heating is delayed in MY20 compared to MRF20 and YSU20 for the June simulation. These results in temperature agree with those found in other studies using other mesoscale models (see e.g., Hu et al., 2010). In addition, doubling the RAMS initial SM has its impact on the forecast of temperature, reproducing its daily evolution properly, specially using YSU40. Fig. 3 also shows that these tendencies are similar when comparing the two selected periods. Finally, considering the VQM station, the observations show a sharp decrease in temperature for the second day of simulation within the 11-12 August period, starting from 12 UTC approximately. The change in temperature due to cloudiness in the area (not shown) is captured by all PBL schemes with different degree of accuracy. This tendency in temperature is simulated by both MY and MRF for the 11

August although the observations do not show this cloudiness, neither shown by YSU (Fig. 3j).

Considering the 10-m wind speed (Fig. 4), there is also a characteristic wind-speed overestimation for the whole day (Gómez et al., 2014a,b). In general, drying the initial SM produces slightly windy results when applying the three PBL schemes. Additionally, the 10-m wind speed is minimally affected between the MY, MRF and YSU using the same initial SM. However, more variability is observed in complex terrain under the precipitation environment (Fig. 4j). On the other hand, the YSU scheme shows, in general, the larger deviations from the observations at nighttime when compared to MY and MRF.

In the case of the wind direction (Fig. 5), RAMS captures the transition between the night land breeze to day-time sea breeze rather well in general. However, YSU and MY20 reproduce a marked nocturnal maritime component compared to the MRF scheme.

4.3. Model comparison with sounding measurements

The upper air model results are compared with the MUR sounding (Fig. 1) for the June period (Fig. 6) and the August period (Fig. 7). Both figures show that RAMS reproduces the essential features of the sea breeze properly. The model captures the switch in wind direction, increase in wind speed and temperature and decrease in relative humidity within the lower boundary representing the sea-breeze layer, as well as the temperature inversion and a marked decrease in wind speed above this layer representing the return current. RAMS reproduces all these essential features of the sea breeze using the different simulations. However, some differences arise. The potential temperature shows that the estimation of the mixing layer height is lowered by moistening the soil for all PBL schemes (Fig. 6a and Fig. 7b). As it was observed near

the surface at 12 UTC, comparing these parameterizations, MRF is colder than YSU, affecting to the estimation of the mixing layer height (Fig. 6a and Fig. 7b). At night (Fig. 6b and Fig. 7a), the differences between both schemes are reduced compared to the results obtained during the day. In this regard, the model is warmer than the observations, specially considering MRF20 and YSU20, within the PBL and at daytime. Additionally, the MY turbulence scheme shows a worse performance than that of MRF and YSU. However, the height of the PBL is not always captured correctly, as shown in Fig. 6a,c and Fig. 7b,d, where the jump of the potential temperature and relative humidity is less pronounced than observed. Considering the mixing efficiency and the entrainment of the different PBL schemes, Fig. 6a shows an steeper slope of the mixing line for MRF and YSU when contrasted to the MY scheme. This is a common characteristic of the non-local schemes and it is related to the higher PBL growth, mainly due to their description of the entrainment, resulting in enhanced mixing compared to local parameterizations (Wisse and Vilà-Guerau de Arellano, 2004). On the other hand, Fig. 6a shows that both MRF and YSU exhibit a far more stable upper mixed layer compared to the observations. Hong et al. (2006) found that the non-local turbulent mixing of heat due to the countergradient effect plays a role in neutralizing the gradient by cooling the lower part of PBL and warming the upper part. Contrasting MRF and YSU PBL schemes, the temperature profiles showed a stable feature in MRF and a near neutral temperature in YSU. Therefore, it seems that the stable upper mixed layer reproduced by the non-local schemes in the current study could also be related to a strong countergradient mixing term. The influence of this term in the vertical profiles has been evaluated here as well by removing it from the original scheme. Similar results to those found by Hong et al. (2006) have been obtained in this case (not shown).

On the other hand, for the 26 June 2011 at 00 UTC, this trend is the opposite using MRF40 and YSU40. Comparing the observed relative humidity with the simulations for the June period (Fig. 6c,d), it is observed that MRF is moister than MY and YSU, with both showing a tendency to under-predict the observations using SM40. In this case, YSU40 is the simulation with the lowest relative humidity within the PBL, while MRF40 performs better. In addition, Fig. 6c shows a secondary maximum in relative humidity near 3,000 m. The observational data recorded on 25 June 2011 at 12 UTC presents a sharp raise above 2,800 m, stabilizing around 3,500 m height. However, the different simulations follow a steady decrease upwards above the PBL, thus providing a significant deviation from the observations. However, for the August period (Fig. 7c,d), MY simulates the low-level relative humidity more suitable, still producing a lower PBL than the one observed. Observations show a far deeper (Fig. 7a) and with a significant higher water content (Fig. 7c) boundary layer compared to model results. In this regard, the model shows more difficulties when forecasting the relative humidity field. Comparing MRF and YSU with MY, it is observed that the non-local schemes reproduce the maximum of the relative humidity within the PBL at a higher height, independently of the SM initialization used. This result is related to the estimation of the mixing height, similar for both the MRF and the YSU schemes and higher than the one obtained for the MY paramaterization. In addition, as it was already observed for the near-surface observations, RAMS shows a windy bias at daytime (F-O>0) starting from the surface (Fig. 6f and Fig. 7e). This trend is maintained aloft and during the night as well (Fig. 6e and Fig. 7f). However, in this case the model shows a better performance for the August period, reproducing the observations accurately. In this regard, the differences between the model and the measurements are greater for the June selected period. Comparing the distinct PBL schemes, it seems that MY is more windy than

MRF and YSU in the lower troposphere, where little contrast is obtained in general aloft. Finally, both simulated periods show an easterly wind in the low atmosphere with a northerly wind aloft at night. It is shown that RAMS is able to capture properly the upper distribution of the wind direction at daytime (Fig. 6g and Fig. 7h) as well as at night (Fig. 6h and Fig. 7g). In this case, some differences are still reproduced between MY, MRF and YSU. Nevertheless, no significant changes are observed in terms of the wind direction.

4.4. Horizontal simulated patterns

Fig. 8 shows the 10-m wind field and the 2-m relative humidity for the 25 June 2011 at 06 UTC. Calm conditions are reproduced by all model simulations, with little differences in the wind flow among the PBL parameterizations and the SM variations. On the contrary, the relative humidity distribution shows significant divergences. Considering the SM modification, YSU is the driest scheme while MY is the moistest one, with MRF in between of both parameterizations. In this regard, differences higher than 30% are observed between MY and YSU. Additionally, moistening the soil has the same effect among the distinct PBL schemes, where all of them show a moister surface layer for SM40 when compared to SM20. The same result is obtained considering the same hour and the other days of simulation (not shown). However, for both simulated periods, it has been found that there is a general trend to decrease the moisture field as the simulation progresses. This result has also been found by Gómez et al. (2015a) for the whole 2011 summer season and using MY20, where the values obtained for the relative humidity were higher for the first day of simulation and the differences between the observations and the model increased for the corresponding forecast two and three days before the specific day of verification. An exception to this general trend is found using the highest initial volumetric SM (SM40) with the MY scheme, but not for MRF

and YSU, specially the latter. In MY40, larger values of relative humidity are still maintained for the second day of simulation, which is particularly significant for those areas with precipitation (the 12 August at 15 UTC over the Teruel Province, not shown).

At 15 UTC (Fig. 9), as for the 06 UTC, the wind field structure in the surface layer is rather alike among the distinct PBL schemes and considering the two initial SM. In addition, and contrary to the results obtained for the 06 UTC, the near-surface relative humidity shows similar results for all the simulations at 15 UTC, but distinguishing between the SM20 and the SM40. In this case, MRF remains close to MY, while YSU is the PBL with the lowest moisture values (Fig. 9f). Although this is the general trend over areas directly affected by the development of the sea-breeze flow (Alicante and Valencia Provinces), some differences arise over areas with precipitation (inland Teruel Province). In this regard, a higher moisture content is simulated by MY for the 11-12 August 2011, specially the 12 August (Fig. 9) due to the development of cloudiness over the area. This result is also reproduced by RAMS the 11 August but with not such a wide extension as in Fig. 9 for the 12 August (not shown). However, the results are qualitatively similar. On the other hand, the wind flow pattern over this area changes among the distinct RAMS runs. Focusing on the MY scheme, it is seen that the sea breeze developed by the MY20 simulation reaches inland areas, while MY40 blocks this development to areas near the coast, extending the inland high moisture towards coastal sites, due to the increased simulated rainfall and cloudiness. This distribution is reproduced by MRF40 as well, but affecting inland areas compared to MY40. However, YSU40 favours the progress of the sea breeze and just a small area of raised relative humidity is reproduced by this scheme and the corresponding SM content. The distribution observed here for the relative humidity has a concrete relation with the latent and sensible heat flux. In this regard, MY40 and MRF40 present values of

sensible heat flux around 50 W/m^2 and even lower over Castellón and Teruel Provinces, reaching coastal areas in the former case, while in other areas values of about 300 W/m^2 and higher are reproduced by the model (not shown).

Finally, considering the SM20 simulations, although a high moisture area is observed inland for MY20, the sea breeze reaches slightly inland areas than those simulated by MRF20 and YSU20. In this case, some differences are observed in the wind field, being MY20 the simulation with the largest penetration of the sea breeze producing high relative humidity inland. However, it seems that MRF20 and YSU20, specially the latter, block the sea breeze development earlier, producing lower relative humidity in those areas unaffected by this wind flow. As previously mentioned, a general trend to decrease the moisture field is obtained using SM20 as the simulation progresses. Thus, the results included here (Fig. 9) for MRF, YSU and MY20 could be related to the differences obtained as the simulation progresses, and the same could be the responsible of the differences between the model and the observations obtained in the simulation for the relative humidity as well as for the precipitation field. In this regard, the deviation observed in the simulation of the moisture pattern by the distinct PBL schemes is translated in the corresponding precipitation distribution. To analyse this meteorological variable, Fig. 10 includes the daily accumulated precipitation for the 12 August 2011 simulated by RAMS and observed, considering the Tropical Rainfall Measuring Mission (TRMM) Multi-Satellite Precipitation Analysis (TMPA) data. In this regard, we have used the TMPA precipitation estimates at 3-hourly temporal resolution (3B42 V7 product) developed and provided by the Mesoscale Atmospheric Processes Laboratory at NASA Goddard Space Flight Center.

The TMPA product show that the precipitation started early in the morning inland. However, no surface data is available over this area to better support the satellite data.

Nevertheless, about noon the precipitation is displaced toward the coast using TMPA, affecting pre-coastal areas located in the Castellón Province in the late afternoon. In this case, the rain gauge data available within the area confirms that the rainfall started between 13 and 14 UTC (VQM weather station) and the late afternoon toward the coast (SEG weather station) (not shown). The observed evolution in the precipitation field is reproduced using MRF40, but with the large amount of precipitation between 12 and 18 UTC. In this case, MRF20 reproduces low precipitation but covering the area observed using the TMPA data. MY40 produces the highest amounts of precipitation. In addition, based on the rainfall trajectory observed using TMPA data, this simulation displaces the greatest amounts inland. However, MY20 follows this trajectory of the precipitation toward the coast. Considering all PBL simulations, YSU20 is the one with the lowest 3-h accumulated values, below 2 mm, lower than those observed.

In terms of the 24-h accumulated rainfall for the 12 August 2011 (Fig. 10), it is seen that the pre-coastal precipitation observed in the Castellón Province is only slightly reproduced by MY20 (Fig. 10a). This simulation reproduces the rainfall distribution properly, but with a significant overestimation inland. However, MY40 produces a great amount of precipitation covering a wider area (Fig. 10d). This high precipitation is also obtained with MRF40 (Fig. 10e), with a lesser extension compared to MY40. Finally, YSU shows absolute amounts of precipitation really close to the observations (Fig. 10f). However, the precipitation distribution is displaced towards the coast in this case, while it is observed inland (Fig. 10g).

Non-local schemes, such as the MRF and YSU parameterizations, tend to produce more vigorous mixing, leading to a more efficient moisture transport up to the higher atmospheric levels. In contrast, local schemes, such as the MY parameterization, produce stronger capping inversions due to a suppressed transport of moisture and heat

to the free atmosphere increasing the convective available potential energy (CAPE), thus affecting to the development of clouds and the rainfall distribution (Wisse and Vilà-Guerau de Arellano, 2004). In this regard, local schemes tend to produce more extreme precipitation rates when simulating convective precipitation events. These results have also been found in the current study. On the other hand, the differences obtained in the cloudy development and the rainfall distribution (Fig. 10), contrasting not only the PBL schemes but also the SM content, are also influencing the mesoscale circulations in the vicinity of the storm, as it was already mentioned above (Fig. 9).

4.5. Vertical simulated patterns

Fig. 11 presents the distribution of the relative humidity and the wind field for a vertical cross section at latitude 40.53 ºN, corresponding to the VQM weather station location, for the 11 August 2011 at 15 UTC. Moistening the soil produces the corresponding effect on all PBL schemes within the lower troposphere. In this regard, a lower mixing height is obtained as a consequence of increasing the SM content. Considering the SM20 simulations, it is found that MY produces a moister mixing layer (Fig. 11a) than MRF (Fig. 11b) and YSU (Fig. 11c). Additionally, the non-local schemes produce a more extensive area with upward circulation, not simulated by MY. As a result, it seems that the non-local parameterizations transport more moisture away from the surface and deposits the moisture at higher levels. In this sense, a stronger vertical mixing is obtained with the MRF and YSU models than using MY, thus leading to a drier PBL at 15 UTC. Thus, differences in vertical mixing would create divergences in the vertical development of the PBL. This is consistent with the results found using other mesoscale models, such as WRF, and other geographical areas (Hong and Pan, 1996; Srinivas et al., 2007; Hu et al., 2010).

Moistening the soil has a significant impact on the PBL structure. In this regard, the vertical motion observed using SM20 is notably reduced by SM40 using all PBL schemes. As a result, the moisture remains trapped within a lower layer and close to the surface layer, thus leading to a reduction in the mixing height. The result is in contrast with that found for SM20, where this moisture is transported upwards. Comparing MY40 (Fig. 11d) with MRF40 (Fig. 11e), the former is moister in the valleys while the later still moves it to higher levels. The pattern reproduced by MRF40 is also seen using YSU40. However, in this case, even lower values of relative humidity are obtained. This reduction in the vertical relative humidity is also observed between MRF and YSU using the initial SM20 content (Fig. 11b,c).

Finally, in order to obtain a better understanding of the vertical structure developed by the different PBL schemes, Fig. 12 and Fig 13 are included. In this regard, Fig. 12 shows the vertical profile of the potential temperature, the water vapor mixing ratio and the horizontal wind speed for the VIL weather station for the 25 June 2011 (left) and the 11 August 2011 (right) at 06 UTC. The different model simulations for SM20 and SM40 separately have similar overall values of vertically integrated potential temperature and moisture. However, significant differences are observed in the lowest troposphere. In this regard, while YSU simulates a clear stratification in the surface layer, MY and MRF, specially the first one, shows a strong inversion layer (Fig. 12a,b) and a sudden change in the moisture field (Fig. 12c,d) both for SM20 and SM40. MRF remains in between the other schemes below 300 m approximately, while MRF is very close to MY upwards. Additionally, YSU produces higher temperatures and less moisture than MY below 1,500 m, as was also obtained for the sounding data at 00 UTC (Fig. 6 and Fig. 7) while all three schemes are very similar to each other upwards. On the other hand, the effect of moistening the soil is well reflected in the lower troposphere through the

temperature and moisture fields. Finally, during nighttime, wind speeds increase with height rapidly in the lowest 500 m approximately and a low-level jet (LLJ) develops considering all parameterizations (Fig. 12e,f). In this regard, since eddy viscosity declines near the surface, all the schemes tend to produce large low-level wind shear. However, some divergences still arise among the three PBL schemes. In addition, MY is the parameterization with the highest wind speed in the lower troposphere. Besides, the wind speed predicted with MY increases more rapidly in the lowest 300 m than that predicted by YSU, resulting in stronger LLJs. As a consequence, during the night, MY predicts a weaker vertical mixing of momentum near the surface than that predicted with YSU. On the other hand, although the effect of moistening the soil is reflected by MY and MRF, YSU20 remains rather similar to YSU40 below 1,000m approximately.

During the day (Fig. 13), SM20 produces similar mixing layer heights over flat terrain than that simulated by SM40 in general. However, in more complex terrain, SM20 leads to a deeper PBL layer (not shown). This behaviour is observed in VIL location (Fig. 1) as well at 12 UTC. However, the opposite trend is obtained at 15 UTC (Fig. 13a,b) for the MY runs. In this case, the vertical wind speed exhibits significant differences over the VIL location in relation to the other sites used in the current study (Fig. 1). Despite the fact that RAMS simulates rather similar vertical wind speeds over flatter terrain and using both SM20 and SM40, there is an opposite tendency in this magnitude over more complex terrain (VQM; Fig. 1), where SM20 simulates an upward motion while SM40 produces a downward circulation. This result is of special significance for the MY runs, but is not obtained using the MRF and YSU schemes. In contrast, considering the VIL site, there is a vertical layer from 500 to 1,500 m approximately, where MY40 produces an ascend vertical motion, while MY20 produces a descending trend (not shown). This result is supported by Fig. 13a,b, where the

general trend of a deeper PBL when drying the soil is reproduced by RAMS using both the MRF and YSU runs. In this regard, YSU produces higher temperatures than MRF, both for SM20 and SM40.

Although the MY runs predict higher temperature and less moisture above 1,500 m than MRF and YSU, they produce lower temperatures and higher moisture below this height. In general, MRF is in between MY and YSU. Once again, Fig. 13c,d shows that the non-local schemes transport more moisture away from the surface and deposits the moisture at a higher level, as it was also indicate in Fig. 12.

Finally, considering the vertical profile for the wind speed, Fig. 13e,f reflect that MY leads to a higher predicted magnitude than that simulated by YSU. This result is obtained considering both initial SM contents. However, although the thermodynamic scalars show that MRF remains in between MY and YSU in terms of heat and moisture, the vertical profiles of wind speed indicates that in this case the MRF scheme produces low wind speed than the other PBL parameterizations, both using SM20 and SM40, as it was also already obtained for the MUR sounding (Fig. 6e).

5. Discussion and conclusions

In the current work, we have implemented two PBL non-local schemes widely used by the scientific community, the MRF and its updated version named YSU, within the RAMS framework. Based on the original formulation by Troen and Mahrt (1986) and developed by Hong and Pan (1996) for the MRF model, we have included the latest modification to this formulation introduced by Noh et al. (2003) and Hong et al. (2006) for the MRF and the YSU parameterizations, as well as the stable boundary layer mixing scheme proposed by Hong (2010).

The sensitivity of the RAMS model to these PBL schemes has been evaluated within an area of the Western Mediterranean coast, specifically focused on mesoscale

circulations, considering that they are the dominant meteorological conditions over this area (Azorin-Molina et al., 2011; Azorin-Molina et al., 2014; Gómez et al., 2014a,b; Gómez et al., 2015a,b). A comprehensive comparison between both PBL schemes has been performed. In addition, the MY parameterization, corresponding to the standard PBL scheme used in the RAMS framework, has been included in the comparison as well.

Thus, two mesoscale circulations have been selected: 25-26 June (at the beginning of the summer) and 11-12 August 2011 (into the summer). Both periods have been chosen because they are a good example of the daytime temperature warm bias obtained in previous studies (Gómez et al., 2014a,b: Gómez et al., 2015a,b). This preceding research was based on the MY20 configuration of the current work. In addition, the sensitivity of the different PBL schemes to the initial SM content has been analysed as well. In this regard, two different initial SM contents have been used, corresponding to a low value (named SM20 here) and a high value (named SM40), doubling the former.

In general, SM20 shows a warmer and dryer PBL than the one observed for all PBL schemes. However, some differences appear among them. In this regard, it has been found that YSU is the warmest and driest scheme while MY is the coldest and moistest one, with MRF in between of both. Thus, the mixing layer height simulated by MY is lower than that reproduced by MRF and YSU. These results are also obtained in the near-surface magnitudes. For example, in terms of 2-m temperature, a significant overestimation is obtained for all PBL schemes during the day. However, greater differences are obtained in relation to the observations using YSU.

Contrasting the results obtained in the current study with those found previously for other areas and using different hosting models for these non-local PBL schemes,

such as the WRF framework, we have detected similarities in the performance of the distinct PBL schemes compared to the observations and among them.

For example, the verification of the 2-m temperature performed by García-Díez et al. (2013) found similar results over the whole Europe as those found by Hu et al. (2010) over Texas and surrounding areas, applying the WRF model to simulate the meteorological conditions of the summer season. In this regard, there is an underestimation of the maximum and minimum temperatures using the MYJ parameterization, derived from the original MY (Janjic, 1994). Although this trend is also obtained using the YSU scheme, the minimum temperature is very well reproduced by this model. These results are also obtained when considering the Iberian Peninsula separately. On the other hand, considering the moisture field, there is a general trend to overestimate the daytime specific humidity, with a less bias using YSU. However, the nighttime specific humidity is closer to the observations. Additionally, MYJ has a tendency to be cooler and moister than YSU for the whole day. The same results have been obtained by Kleczek et al. (2014) within the summer season. Furthermore, this temperature cold bias has also been obtained by Hernández-Ceballos et al. (2013) for the southwestern Iberian Peninsula under mesoscale circulations using the MRF scheme within the WRF model.

In the current study, based on the RAMS model, similar results as those described are obtained when comparing MY and YSU in terms of the 2-m temperature. However, contrasting these schemes, as well as the MRF model, with the observations, a general tendency to overestimate the maximum temperature is obtained for the SM20 simulations, as a notable difference with the above mentioned studies. This warm bias in temperature was also detected using the WRF model for a single day from the Cooperative Atmosphere-Surface Exchange Study (CASES-99) field program, held in

Kansas (USA), and corresponding to the month of October 1999 (Shin and Hong, 2011).

As it was suggested by Hu et al., (2010), the daytime temperature biases may be caused by errors in SM. Although no further analysis was addressed in this direction there, a comprehensive evaluation of the PBL schemes and their relevant surface-layer schemes was conducted. In contrast, the sensitivity of the three PBL schemes to this parameter has been considered in the current work. In this sense, doubling the original SM content in the RAMS initialization has a significant and positive impact towards the reduction of the temperature field, specially during the day. With the SM40 simulation, YSU seems to reproduce better the maximum temperature, while the minimum is still overestimated in general.

Comparing the vertical profiles, there is a general trend to simulate a colder and moister and less mixed PBL than observed using the local and non-local PBL schemes within the WRF model (see e.g. Hu et al., 2010; García-Díez et al., 2013; Kleczek et al., 2014). However, the study by Shin and Hong (2011) shows a similar structure as the one found in the current work using RAMS. In this regard, there is a tendency to simulate a warmer and dryer PBL than the one observed. In addition, it has been found that moistening the soil has a positive impact on the reproduction of both the observed vertical structure and the surface layer patterns. However, the significant overestimation of the near-surface wind speed over flatter terrain and obtained using SM20 continues using SM40, although the bias is slightly reduced. Thus, more efforts should be addressed with the aim of reducing these differences.

In general, the YSU scheme leads to a higher temperature and a lower moisture than MY and MRF during daytime due to a stronger vertical mixing. This process causes stronger entrainment at the top of PBL, which helps to warm and dry the PBL

(Hu et al., 2010). Additionally, YSU also shows an enhanced mixing during nighttime, that translates into a higher temperature and a lower moisture than MRF and MY. This has been found independently of the initial SM content used. In terms of processes, it has been found that YSU and MRF produce an early heating than MY, specially using a low SM content.

In previous studies with the original MRF scheme on RAMS, it was observed that this model suffers from a substantial cold and humid bias in the daytime boundary layer, which results in an underestimation of the diurnal cycle at screen level (Tolt et al., 2009; Steeneveld et al., 2011). In the current study, we have found in general the opposite trend for the Western Mediterranean coast within the summer season.

It is well known that if the difference between the schemes were exclusively caused by mixing within the lowest levels of the atmosphere, the scheme that produces the moistest daytime surface conditions (MY) should also produce the warmest daytime surface conditions, but it does not (Hu et al., 2010). However, entrainment plays a key role here. While air originating from the surface layer during the daytime typically has both higher potential temperature and greater moisture than the average air within the PBL, air entrained from above the PBL has higher potential temperature but less moisture than typical PBL air. Consequently, errors in entrainment would lead to oppositely signed biases in PBL temperature and moisture (Hu et al., 2010). In this regard, MY produces lower PBL heights than both MRF and YSU, thus suggesting less entrainment of free-tropospheric air into the PBL. Besides, although the main difference between MRF and YSU is the parameterization of the entrainment, significant differences are found in the vertical development of the PBL, specially during the day. Therefore, the role of entrainment is highlighted.

Additionally, comparing SM20 with SM40 it has been found that the former has a tendency to simulate deeper PBL mixing layers than the latter. In this sense, the mixing layer height over more complex terrain is decreased by SM40 in relation to the one obtained by SM20 for all PBL parameterizations. However, it seems that it is necessary to increase the initial SM content in order to better represent the observations during the day. In this regard, the non-local schemes are more favourable under unstable conditions, while the local TKE closure scheme (MY) seems to reproduce more properly the observations at nighttime, under stable conditions. These results suggest that the representation of surface variables is still uncertain even using the state-of-the-art PBL schemes, especially under stable conditions (Shin and Hong, 2011).

Finally, the wind speed presents a significant overestimation over flatter terrain for all PBL schemes during day time, although this bias is notably reduced in complex terrain. In addition, YSU shows a general windy tendency at nighttime when compared to the observations as well as the MRF and MY models. The systematic differences of wind speeds in the PBL found during the day may have important implications for the simulated horizontal dispersion of pollutants in air quality modelling (Hu et al., 2010). It is well known that an accurate depiction of meteorological conditions, especially within the PBL, is important not only for air pollution modelling (Hu et al., 2010) but also in studies of the carbon budget using modelling. Thus, different efforts have been made in order to better simulate the boundary layer in different versions of the RAMS model, with a special emphasize on the entrainment parameterization (McGrath-Spangler et al., 2009; McGrath-Spangler et al., 2010; Tolk et al., 2009). For instance, Tolk et al. (2009) found that the simulations with the RAMS MRF scheme showed a better performance than the standard MY scheme, confirming the importance of the parameterizations of turbulence and entrainment for the simulation of the atmospheric

profiles. Finally, McGrath-Spangler et al. (2010) implemented an entrainment parameterization in the RAMS model, and found that the enhancement of entrainment effects increased the model estimate of the PBL depth in the simulation of the corresponding weather conditions.

Thus, the results obtained in the current work applying the RAMS model are consistent with those found in previous studies using other mesoscale models. However, some differences have been highlighted in relation to the bias of the simulation trends compared to the observations. Although further investigation should be performed in the future with the aim of improving the RAMS forecasts under mesoscale circulations, we have specially shown here the overestimation of the near-surface and vertical wind speed over flatter terrain, it is very encouraging to notice the improvement produced in the model results in the current study. On the one hand, with the introduction of an explicit treatment of the entrainment, and on the other hand, considering a moister soil for the initialization of the model.

Acknowledgement

This work has been funded by the Regional Government of Valencia through the project PROMETEOII/2014/086 and by the Spanish Ministerio de Economía y Competitividad through the projects CGL2013-46862-C02-1-P and CGL2015-64268-R. NCEP is acknowledged for providing the FNL analysis data for RAMS initialization. National Centers for Environmental Prediction/National Weather Service/NOAA/U.S. Department of Commerce (2000): NCEP FNL Operational Model Global Tropospheric Analyses, continuing from July 1999. Research Data Archive at the National Center for Atmospheric Research, Computational and Information Systems Laboratory. Dataset. http://rda.ucar.edu/datasets/ds083.2. Accessed 25 August 2014. The authors acknowledge the Atmospheric Soundings portal of the University of Wyoming

(http://weather.uwyo.edu/upperair/sounding.html) for providing the radiosonde data. Additionally, we would like to thank the Spanish Ministry of Agriculture, Food and Environment for making the surface observations available through the SIAR system. Finally, the TMPA data were provided by the NASA Goddard Space Flight Center's Mesoscale Atmospheric Processes Laboratory and Precipitation Processing System (PPS), which develop and compute the TMPA as a contribution to TRMM, and archived at the NASA Goddard Earth Sciences Data and Information Services Center (GES DISC).

References

Angevine, W.M., Bazile, E., Legain, D., Pino, D., 2014. Land surface spinup for episodic modeling. Atmos. Chem. Phys. 14 (15), 8165–8172. http://dx.doi.org/10.5194/acp-14-8165-2014.

Azorin-Molina, C., Chen, D., Tijm, S., Baldi, M., 2011. A multi-year study of sea breezes in a Mediterranean coastal site: Alicante (Spain). Int. J. Climatol. 31, 468–486. http://dx.doi.org/10.1002/joc.2064.

Azorin-Molina, C., Tijm, S., Ebert, E.E., Vicente-Serrano, S.M., Estrela, M.J., 2014. Sea breeze thunderstorms in the eastern Iberian Peninsula. Neighborhood verification of HIRLAM and HARMONIE precipitation forecasts. Atmos. Res. 139, 101-115. http://dx.doi.org/10.1016/j.atmosres.2014.01.010.

Braun, S., Tao, W., 2000. Sensitivity of high-resolution simulations of hurricane Bob (1991) to planetary boundary layer parameterizations. Mon. Weather Rev. 128(12), 3941–3961.

Borge, R., Alexandrov, V., del Vas, J.J., Lumbreras, J., Rodríguez, E., 2008. A comprehensive sensitivity analysis of the WRF model for air quality applications over the Iberian Peninsula. Atmos. Environ. 42, 8560–8574.

Challa, V.S., Indracanti, J., Rabarison, M.K., Patrick, C., Baham, J.M., Young, J., Hughes, R., Hardy, M.G., Swanier, S.J., Yerramilli, A., 2009. A simulation study of mesoscale coastal circulations in Mississippi Gulf coast. Atmos. Res. 91(1), 9-25.

Chen, C., Cotton, W.R., 1983. A one-dimensional simulation of the stratocumulus-capped mixed layer. Boundary-Layer Meteorol. 25, 289–321.

Cotton, W.R., Pielke, R.A.S., Walko, R.L., Liston, G.E., Tremback, C.J., Jiang, H., McAnelly, R.L., Harrington, J.Y., Nicholls, M.E., Carrio, G.G., McFadden, J.P., 2003.

RAMS 2001: Current status and future directions. Meteorol. Atmos. Phys. 82 (1-4), 5-29.

Cuxart, J., Holtslag, A.A.M., Beare, R.J., Bazile, E., Beljaars, A., Cheng, A., Conangla, L., Ek, M., Freedman, F., Hamdi, R., Kerstein, A., Kitagawa, H., Lenderink, G., Lewellen, D., Mailhot, J., Mauritsen, T., Perov, V., Schayes, G., Steeneveld, G-J., Svensson, G., Taylor, P., Weng, W., Wunsch, S., Xu, K-M., 2006. Single-column model intercomparison for a stably stratified atmospheric boundary layer. Boundary-Layer Meteorol. 118, 273–303.

Daniels, E.E., Hutjes, R.W.A., Lenderink, G., Ronda, R.J., Holtslag, A.A.M., 2015. Land Surface Feedbacks on Spring Precipitation in the Netherlands. J. Hydrometeorol. 16, 232–243. http://dx.doi.org/10.1175/JHM-D-14-0072.1.

Deng, A., Stauffer, D., 2006. On improving 4-km mesoscale model simulations. J. Appl. Meteorol. 45(3), 361–381.

García-Díez, M., Fernández, J., Fita, L., Yagüe, C., 2013. Seasonal dependence of WRF model biases and sensitivity to PBL schemes over Europe. Q. J. R. Meteorol. Soc. 139(671), 501–514.

Gómez, I., Caselles, V., Estrela, M.J., 2014a. Real-time weather forecasting in the Western Mediterranean Basin: An application of the RAMS model. Atmos. Res. 139, 71-89. http://dx.doi.org/10.1016/j.atmosres.2014.01.011.

Gómez, I., Caselles, V., Estrela, M.J., Niclòs, R., 2014b. RAMS-forecasts comparison of typical summer atmospheric conditions over the Western Mediterranean coast. Atmos. Res. 145-146, 130-151. http://dx.doi.org/10.1016/j.atmosres.2014.03.018.

Gómez, I., Estrela, M.J., Caselles, V., 2015a. Verification of the RAMS-based operational weather forecast system in the Valencia Region: a seasonal comparison. Nat. Hazards 75(2), 1941-1958. http://dx.doi.org/10.1007/s11069-014-1408-9.

Gómez, I., Caselles, V., Estrela, M.J., 2015b. Impacts of soil moisture content on simulated mesoscale circulations during the summer over eastern Spain. Atmos. Res. 164-165, 9-26. http://dx.doi.org/10.1016/j.atmosres.2015.04.015.

Hariprasad, K.B.R.R., Srinivas, C.V., Bagavath Singh, A., Vijaya Bhaskara Rao, S., Baskaran, R., Venkatraman, B., 2014. Numerical simulation and intercomparison of boundary layer structure with different PBL schemes in WRF using experimental observations at a tropical site. Atmos. Res. 145-146, 27-44. http://dx.doi.org/10.1016/j.atmosres.2014.03.023.

Hernández-Ceballos, M.A., Adame, J.A., Bolívar, J.P., De la Morena, B.A., 2013. A mesoscale simulation of coastal circulation in the Guadalquivir valley (southwestern Iberian Peninsula) using the WRF-ARW model. Atmos. Res. 124, 1-20. http://dx.doi.org/10.1016/j.atmosres.2012.12.002.

Hong, S-Y., Pan, H-L,. 1996. Nonlocal boundary layer vertical diffusion in a medium-range forecast model. Mon. Weather Rev. 124(10), 2322–2339.

Hong, S., Noh, Y., Dudhia, J., 2006. A new vertical diffusion package with an explicit treatment of entrainment processes. Mon. Weather Rev. 134(9), 2318–2341.

Hong, S-Y., 2010. A new stable boundary-layer mixing scheme and its impact on the simulated East Asian summer monsoon. Q. J. R. Meteorol. Soc. 136, 1481–1496.

Hu, X-M., Nielsen-Gammon, J.W., Zhang, F., 2010. Evaluation of three planetary boundary layer schemes in the WRF model. J. Appl. Meteorol. Climatol. 49(9), 1831–1844.

Janjic, Z.A., 1994. The step-mountain ETA coordinate model: further development of the convection, viscous sublayer and turbulence closure scheme. Mon. Weather Rev. 122(5), 927–945.

Kalverla, P.C., Duine, G.J., Steeneveld, G.J., Hedde, T., 2016. Evaluation of the Weather Research and Forecasting model in the Durance Valley complex terrain during the KASCADE field campaign. J. Appl. Meteorol. Climatol. http://dx.doi.org/10.1175/JAMC-D-15-0258.1.

Kleczek, M.A., Steeneveld, G.J., Holtslag, A.A.M., 2014. Evaluation of the Weather Research and Forecasting Mesoscale Model for GABLS3: Impact of Boundary-Layer Schemes, Boundary Conditions and Spin-Up. Boundary-Layer Meteorol. 152, 213-243. http://dx.doi.org/10.1007/s10546-014-9925-3.

Louis, J.F., 1979. A parametric model of vertical eddy fluxes in the atmosphere. Boundary-Layer Meteorol. 17, 187–202.

McGrath-Spangler, E.L., Scott Denning, A., Corbin, K.D., Baker, I.T., 2009. Sensitivity of Land-Atmosphere Exchanges to Overshooting PBL Thermals in an Idealized Coupled Model. J. Adv. Model. Earth Sy. 1, 14.

McGrath-Spangler, E.L., Scott Denning, A., 2010. Impact of entrainment from overshooting thermals on land–atmosphere interactions during summer 1999. Tellus Ser. B 62, 441–454.

Mellor, G., Yamada, T., 1982. Development of a turbulence closure model for geophysical fluid problems. Rev. Geophys. 20, 851-875.

Miao, J-F., Chen, D., Wyser, K., Borne, K., Lindgren, J., Strandevall, M.K.S., Thorsson, S., Achberger, C., Almkvist, E., 2008. Evaluation of MM5 mesoscale model at local scale for air quality applications over the Swedish west coast: Influence of PBL and LSM parameterizations. Meteorol. Atmos. Phys. 99, 77-103.

Miao, J-F., Wyser, K., Chen, D., Ritchie, H., 2009. Impacts of boundary layer turbulence and land surface process parameterizations on simulated sea breeze characteristics. Ann. Geophys. 27, 2303-2320.

Millán, M.M., Salvador, R., Mantilla, E., Kallos, G., 1997. Photooxidants dynamics in the Mediterranean basin in summer: Results from European research projects. J. Geophys. Res. 102(D7), 8811–8823.

Millán, M.M., Mantilla, E., Salvador, R., Carratalá, A., Sanz, M.J., Alonso, L., Gangoiti, G., Navazo, M., 2000. Ozone cycles in the Western Mediterranean basin: Interpretation of monitoring data in complex coastal terrain. J. Appl. Meteorol. 39 (4), 487–508.

Molinari, J., 1985. A general form of kuo's cumulus parameterization. Mon. Weather Rev. 113, 1411-1416.

Nakanishi, M., Niino, H., 2004. An improved Mellor-Yamada level-3 model with condensation physics: its design and verification. Boundary-Layer Meteorol. 112, 1–31.

NCEP, 2014. National Centers for Environmental Prediction/National Weather Service/NOAA/U.S. Department of Commerce (2000): NCEP FNL Operational Model Global Tropospheric Analyses, continuing from July 1999. Research Data Archive at the National Center for Atmospheric Research, Computational and Information Systems Laboratory. Dataset. http://rda.ucar.edu/datasets/ds083.2. Accessed 25 August 2014.

Noh, Y., Cheon, W-G., Hong, S-Y., 2003. Improvement of the K-profile model for the planetary boundary layer based on large eddy simulation data. Boundary-Layer Meteorol. 107, 401–427.

Pielke Sr., R.A., 2013. Mesoscale meteorological modeling. 3rd Edition. Academic Press, San Diego, CA, 760 pp.

Shin, H., Hong, S-Y., 2011. Intercomparison of planetary boundary-layer parametrizations in the WRF model for a single day from CASES-99. Boundary-Layer Meteorol. 139(2), 261–281.

Skamarock, W.C., Klemp, J.B., Dudhia, J., Gill, D.O., Barker, D.M., Duda, M.G., Huang, X.Y., Wang, W., Powers, J.G., 2008. A Description of the Advanced Research

WRF Version 3. NCAR Technical Note, NCAR/TN-475+STR. Mesoscale and Microscale Meteorology Division, National Center for Atmospheric Research, Boulder, CO, USA.

Srinivas, C.V., Venkatesan, R., Singh, A.B., 2007. Sensitivity of mesoscale simulations of land-sea breeze to boundary layer turbulence parameterization. Atmos. Environ. 41, 2534–2548.

Steeneveld, G.J., Vilà-Guerau de Arellano, J., Holtslag, A., Mauritsen, A.A.M., Svensson, G., de Bruijn, E.I.F., 2008. Evaluation of limited-area models for the representation of the diurnal cycle and contrasting nights in CASES-99. J. Appl. Meteorol. Climatol. 47(3), 869–887.

Steeneveld, G.J., Tolk, L.F., Moene, A.F., Hartogensis, O.K., Peters, W., Holtslag, A.A.M., 2011. Confronting the WRF and RAMS mesoscale models with innovative observations in the Netherlands: evaluating the boundary layer heat budget. J. Geophys. Res. 116(D23), D23114.

Tolk, L.F., Peters, W., Meesters, A.G.C.A., Groenendijk, M., Vermeulen, A.T., Steeneveld, G.J., Dolman, A.J., 2009. Modelling regional scale surface fluxes, meteorology and CO_2 mixing ratios for the Cabauw tower in the Netherlands. Biogeosciences 6, 2265–2280.

Troen, I.B., Mahrt, L., 1986. A simple model of the atmospheric boundary layer: sensitivity to surface evaporation. Boundary-Layer Meteorol. 37(1–2), 129–148.

Walko, R.L., Band, L.E., Baron, J., Kittel, T.G.F., Lammers, R., Lee, T.J., Ojima, D., Pielke, R.A., Taylor, C., Tague, C., Tremback, C.J., Vidale, P.L., 2000. Coupled atmospheric-biophysics-hydrology models for environmental modeling. J. Appl. Meteorol. 39, 931-944.

Wisse, J.S.P., Vilà-Guerau de Arellano, J., 2004. Analysis of the role of the planetary

boundary layer schemes during a severe convective storm. Ann. Geophys. 22, 1861-1874. http://dx.doi.org/10.5194/angeo-22-1861-2004.

Zhong, S., In, H., Clements, C., 2007. Impact of turbulence, land surface, and radiation parameterizations on simulated boundary layer properties in a coastal environment. J. Geophys. Res. 112, D13110.

Figure captions

Fig. 1. Model domain configuration and orography (m) on domain D1. Weather station locations are indicated within the finer domain (D3) combined to the corresponding orography.

Fig. 2. Sea level pressure (hPa, solid line), geopotential height (gpm, shaded color) and temperature in ºC (dashed line) at 500 hPa from FNL global model at 12 UTC on 25 June (a), 26 June (b), 11 August (c) and 12 August (d) 2011.

Fig. 3. Observed (black) and simulated 2-m temperature (ºC) time series, for different surface weather stations during the June period (left): SAN (a), SEG (c), XAT (e), VIL (g), VQM (i), and the August period (right): SAN (b), SEG (d), XAT (f), VIL (h), VQM (j).

Fig. 4. Same as Fig. 3, but for the 10-m wind speed (m/s).

Fig. 5. Same as Fig. 3, but for the near-surface wind direction (º).

Fig. 6. Observed (black) and simulated vertical profiles for the MUR sounding station and for the June period. 25 June at 12 UTC (left): potential temperature, (K; a), relative humidity (%; c), wind speed (m/s; e) and wind direction (º; g). 26 June at 00 UTC (right): potential temperature, (K; b), relative humidity (%; d), wind speed (m/s; f) and wind direction (º; h).

Fig. 7. Same as Fig. 6, but for the August period: 11 August at 00 UTC (left) and 11 August at 12 UTC (right).

Fig. 8. Comparison of simulated near-surface wind field (scale: 10 m/s) and relative humidity (%) on domain D3 on 25 June 2011 at 06 UTC: MY20 (a), MRF20 (b), YSU20 (c), MY40 (d), MRF40 (e), YSU (f).

Fig. 9. Same as Fig, 8, but on 12 August 2011 at 15 UTC.

Fig. 10. 24-h observed and simulated accumulated precipitation (mm) for the 12 August 2011: MY20 (a), MRF20 (b), YSU20 (c), MY40 (d), MRF40 (e), YSU (f), Observations (TMPA; g).

Fig. 11. Vertical variation of the simulated wind field (m/s) and relative humidity (%) for a cross-section at latitude 40.53º N on 25 June 2011 at 15 UTC: MY20 (a), MRF20 (b), YSU20 (c), MY40 (d), MRF40 (e), YSU (f).

Fig. 12. Comparison of simulated vertical profiles for VIL station on 25 June 2011 at 06 UTC (left): potential temperature, (K; a), water vapor mixing ratio (g/Kg; c) and wind speed (m/s; e), and on 11 August 2011 at 06 UTC (right): potential temperature, (K; b), water vapor mixing ratio (g/Kg; d) and wind speed (m/s; f).

Fig. 13. Same as Fig. 12, but on 25 June 2011 at 15 UTC (left) and 11 August 2011 at 15 UTC (right).

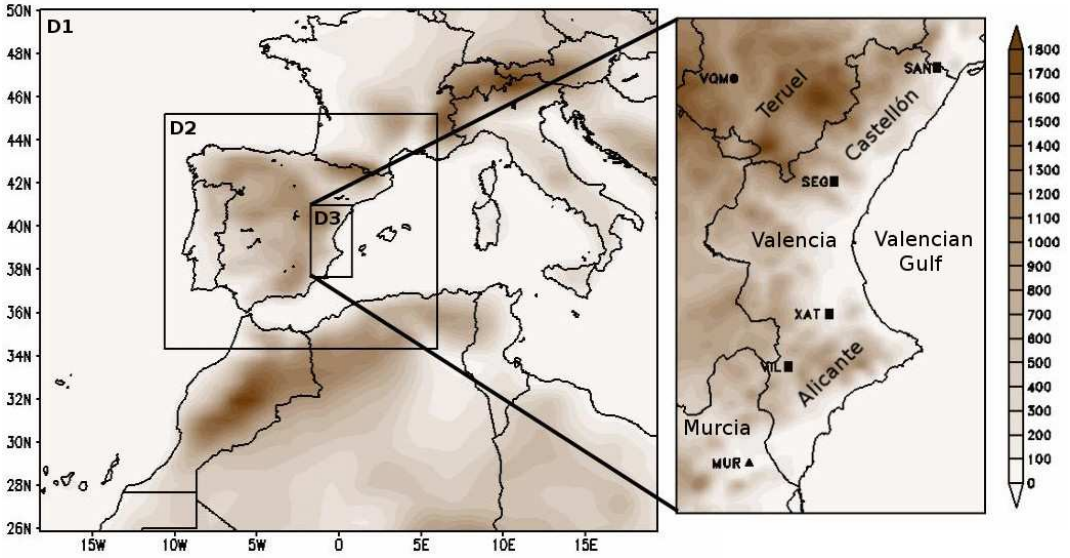

Figure 1

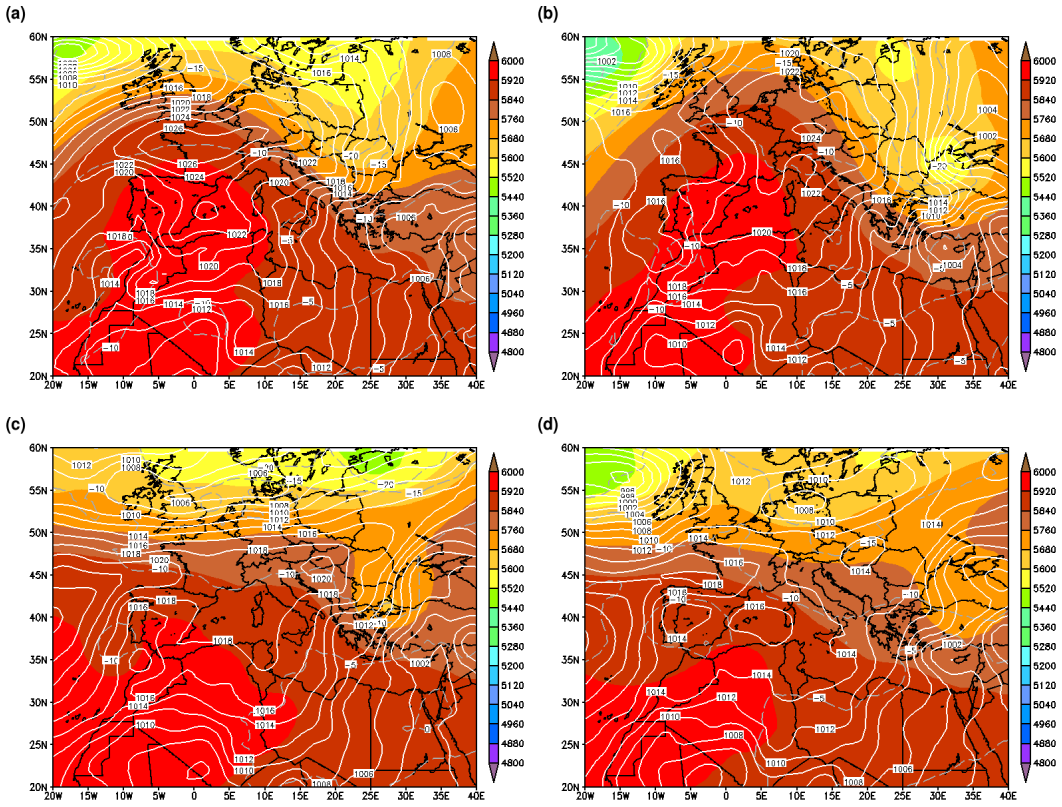

Figure 2

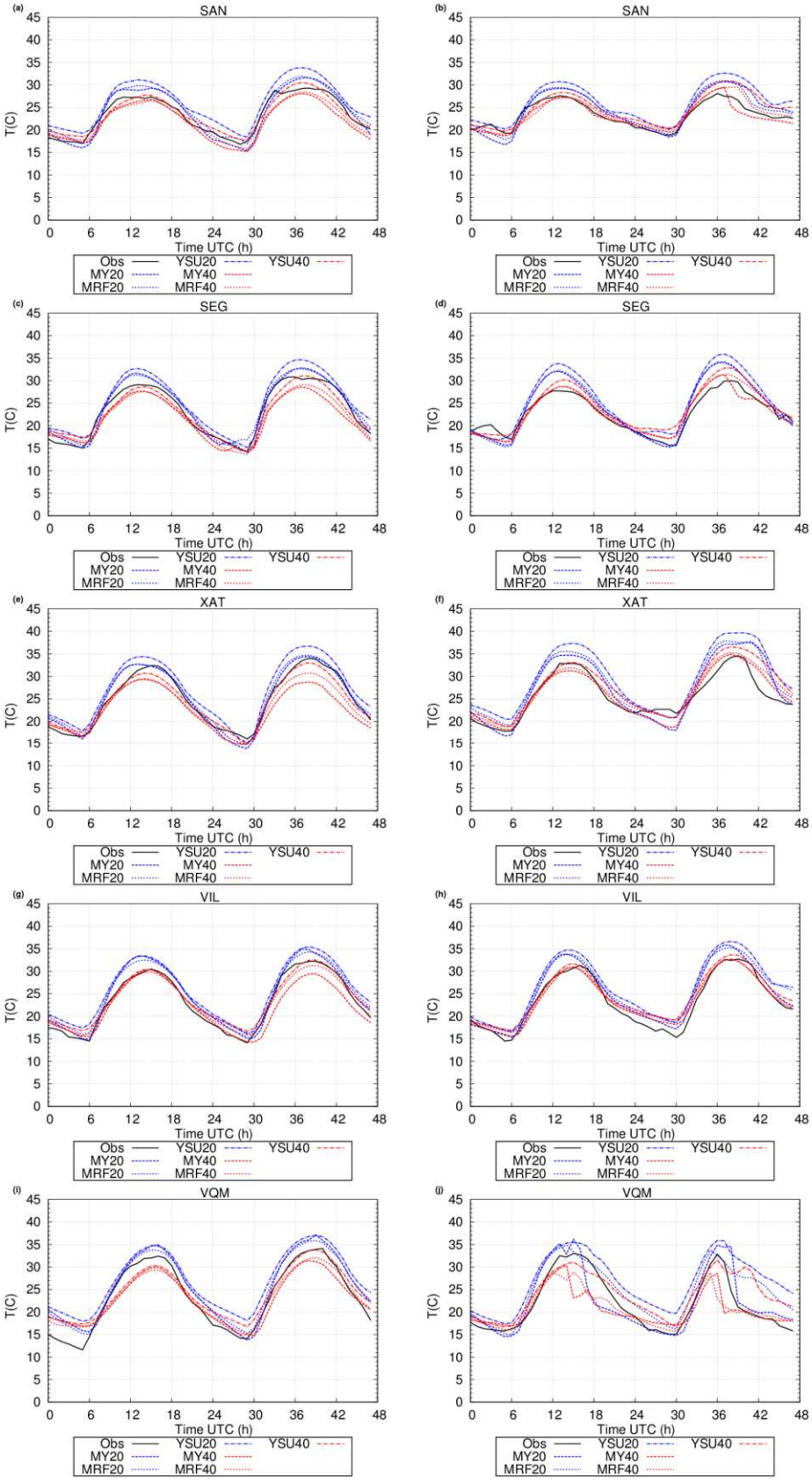

Figure 3

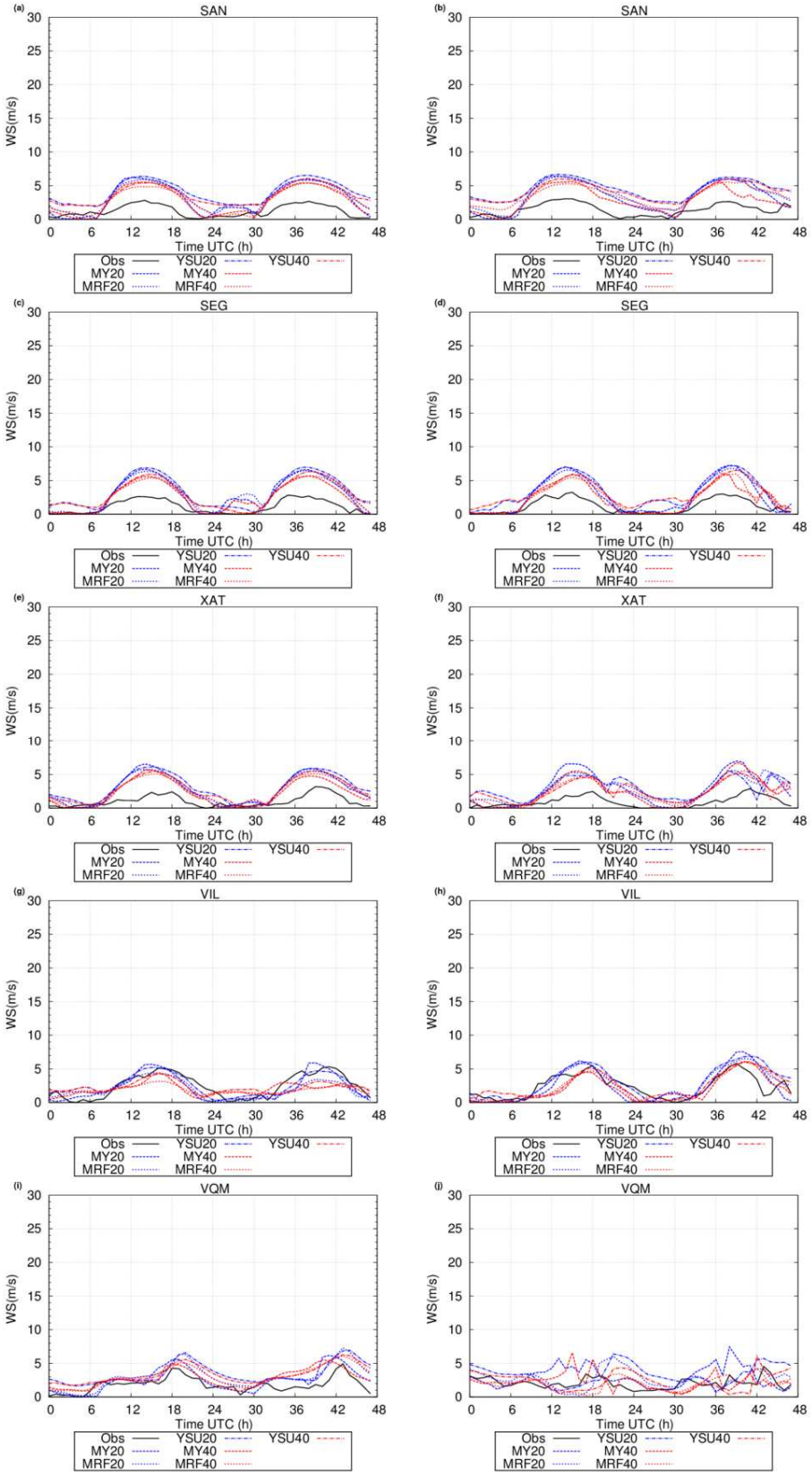

Figure 4

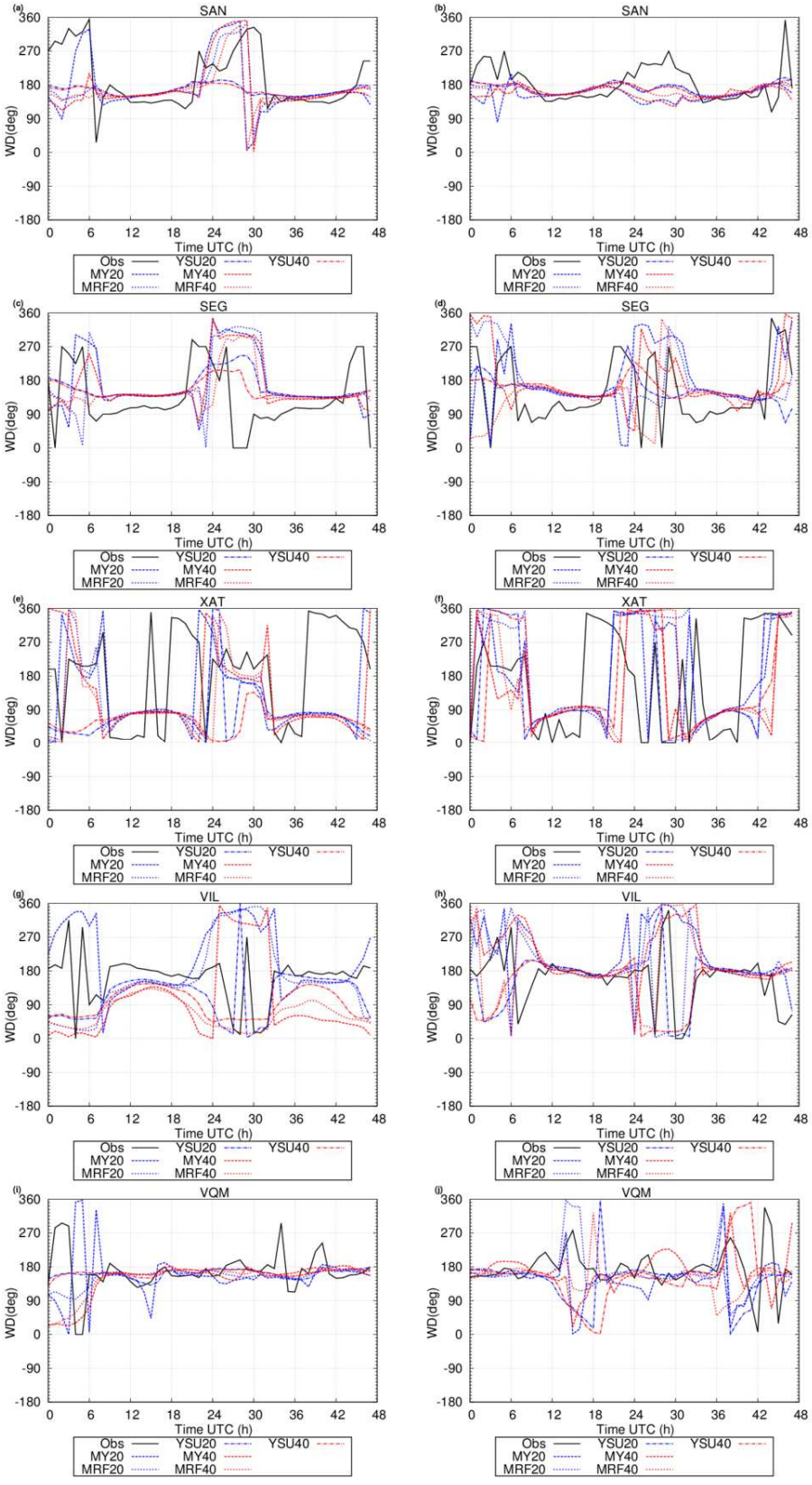

Figure 5

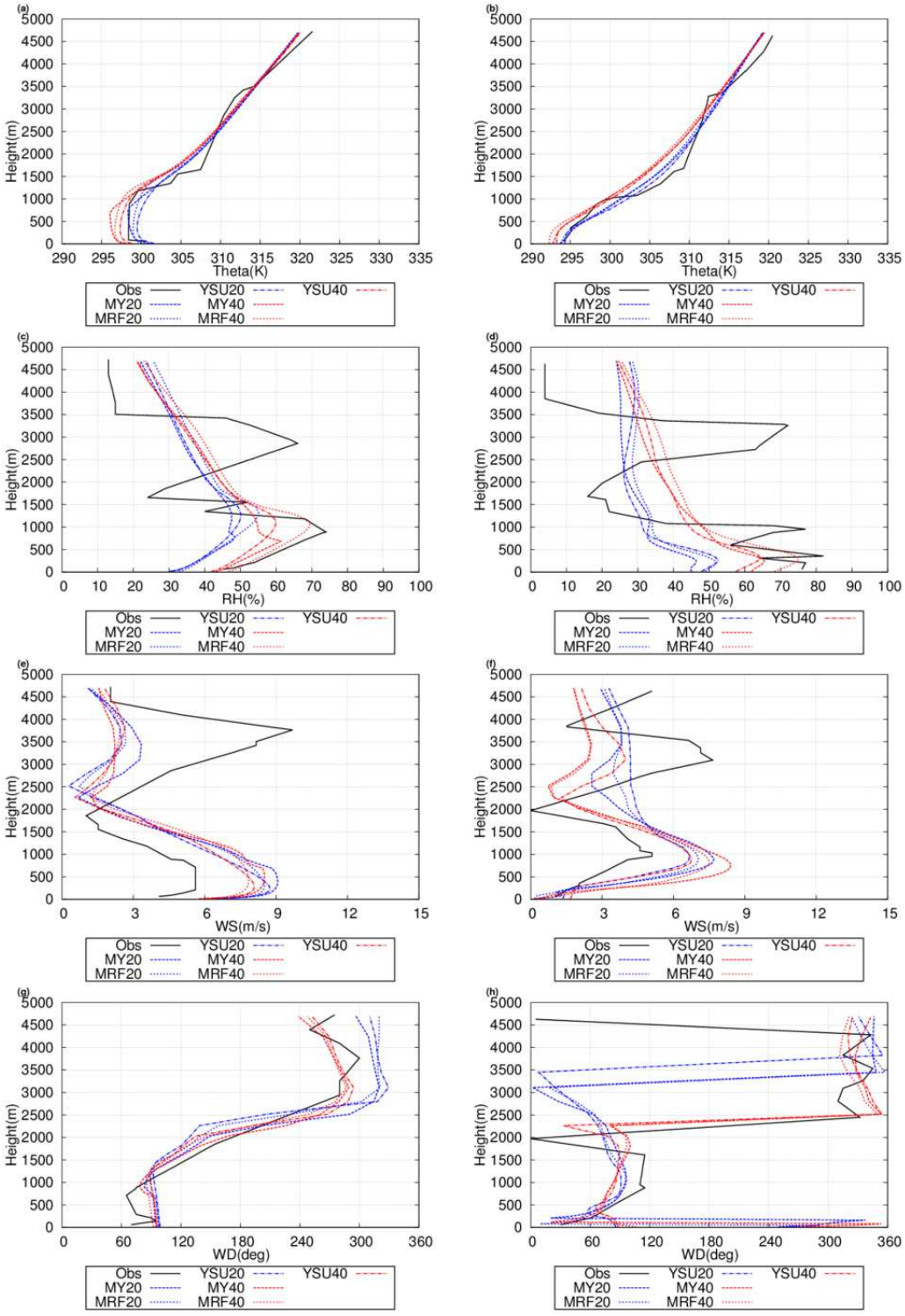

Figure 6

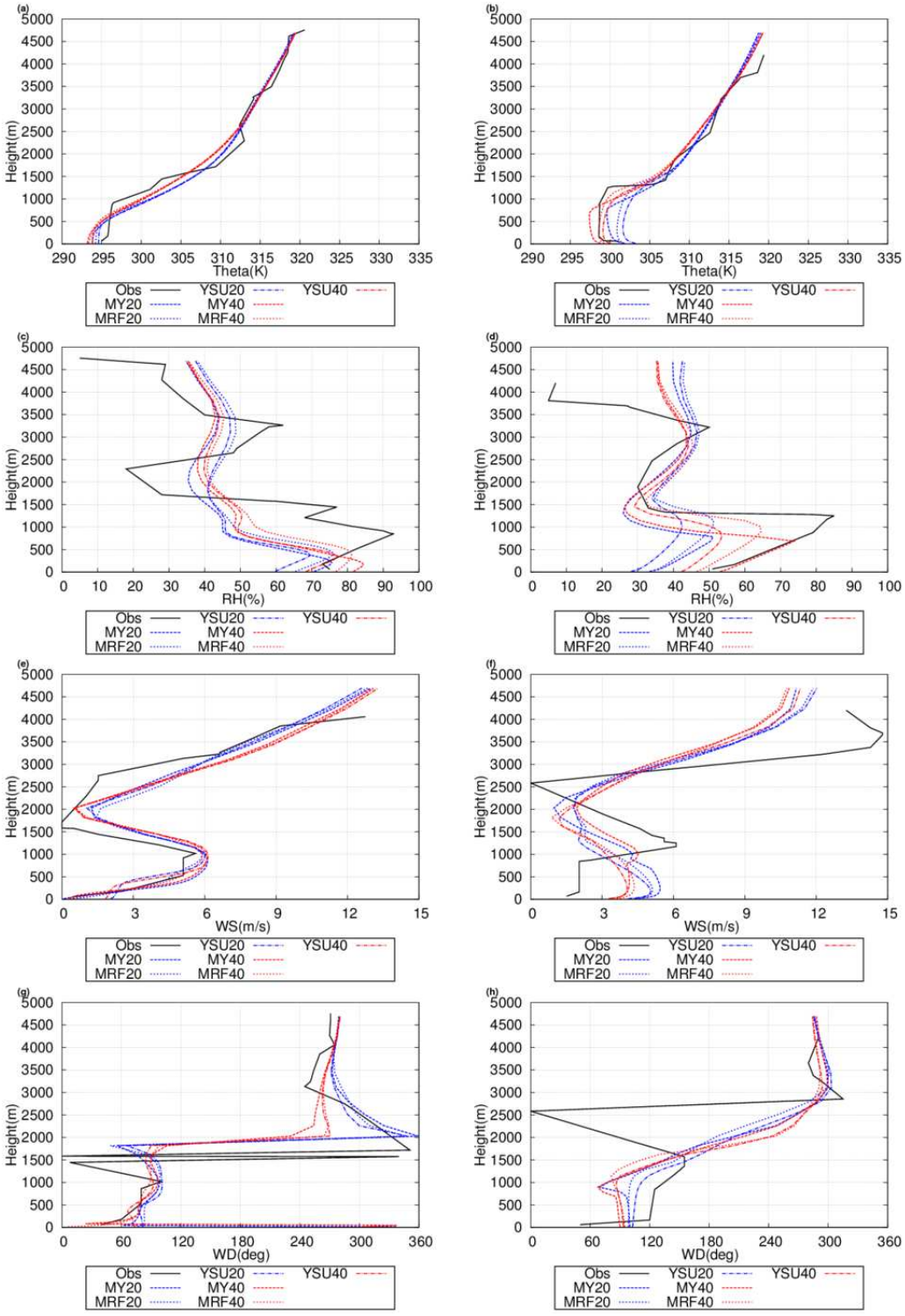

Figure 7

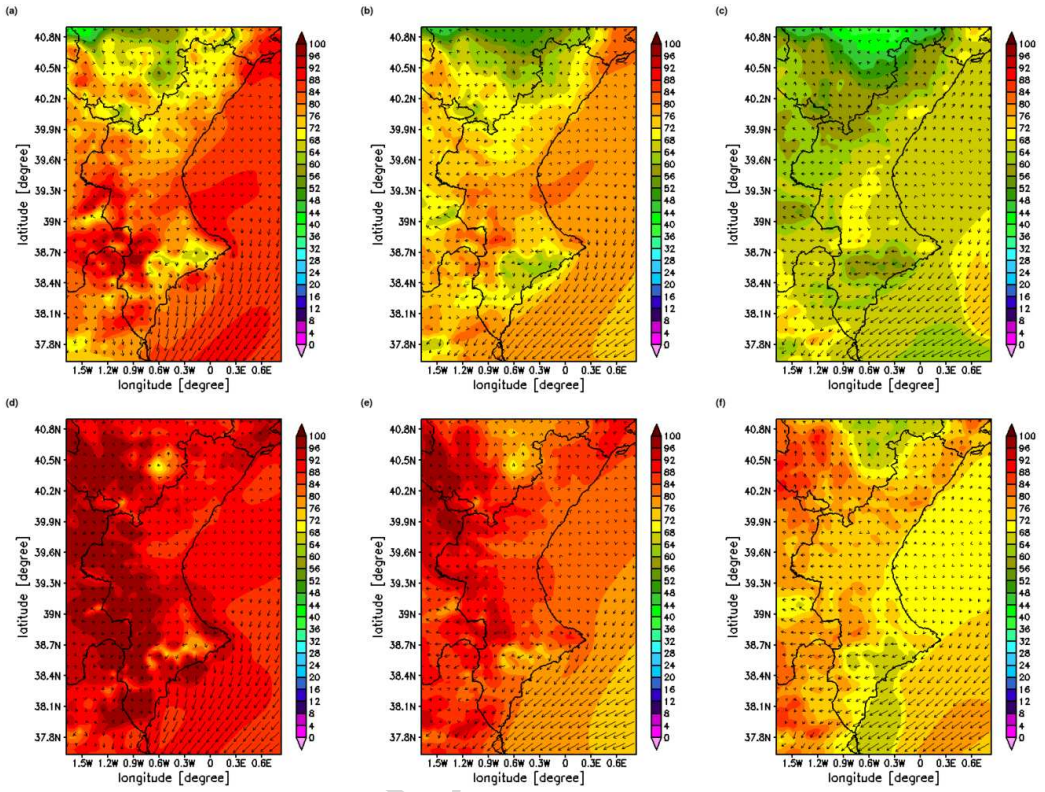

Figure 8

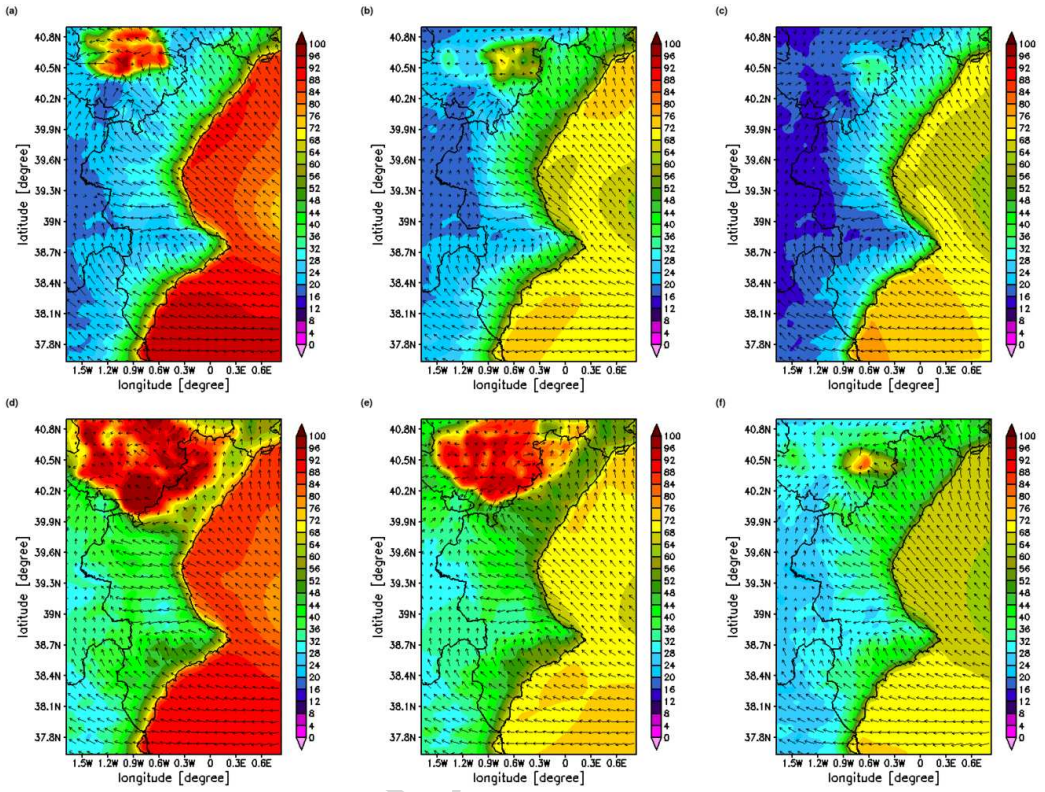

Figure 9

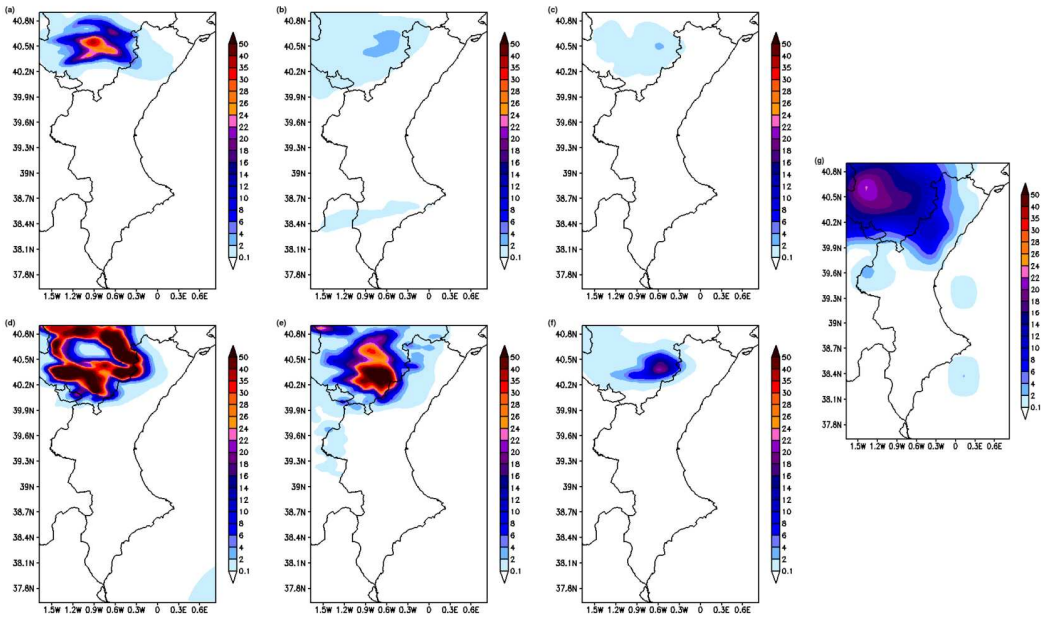

Figure 10

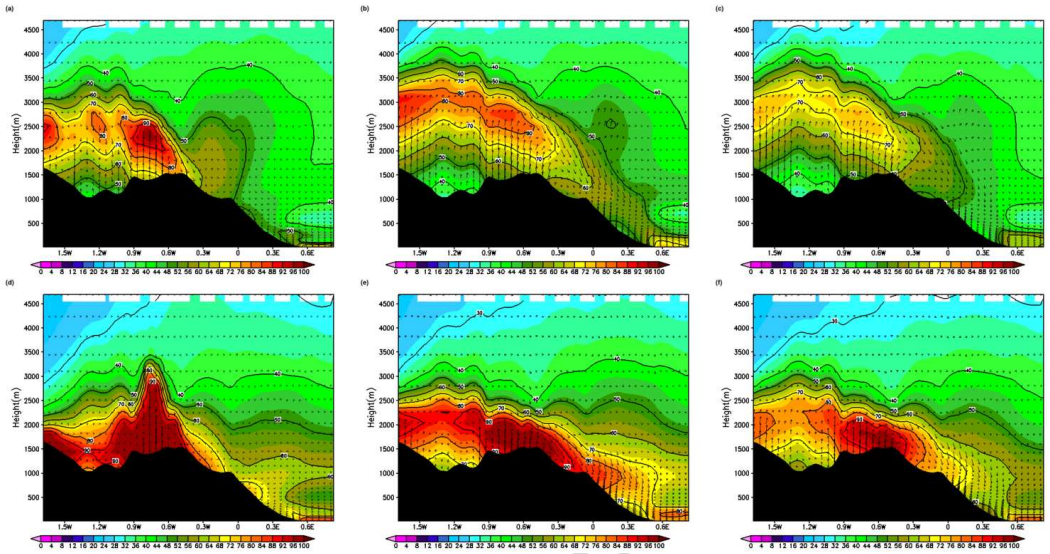

Figure 11

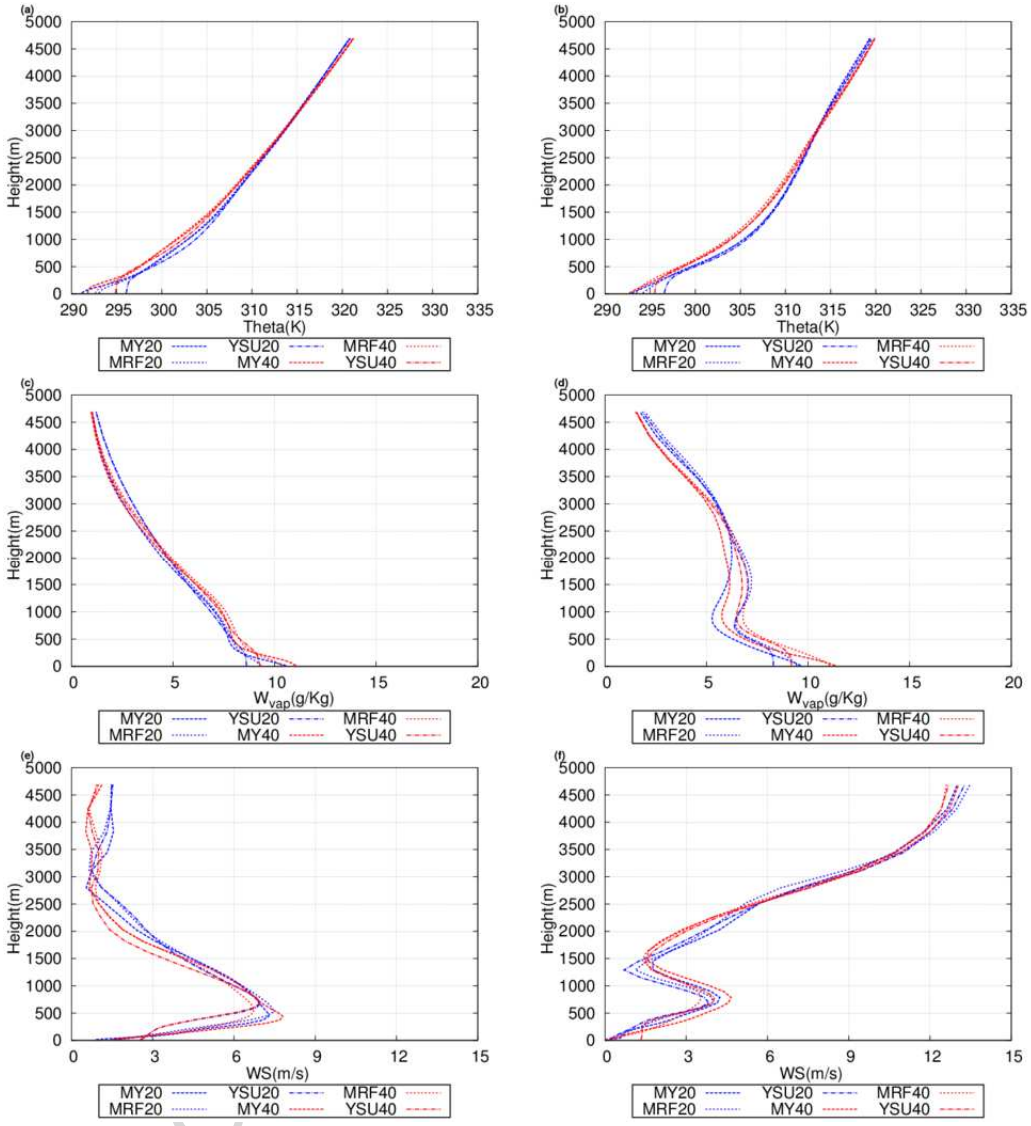

Figure 12

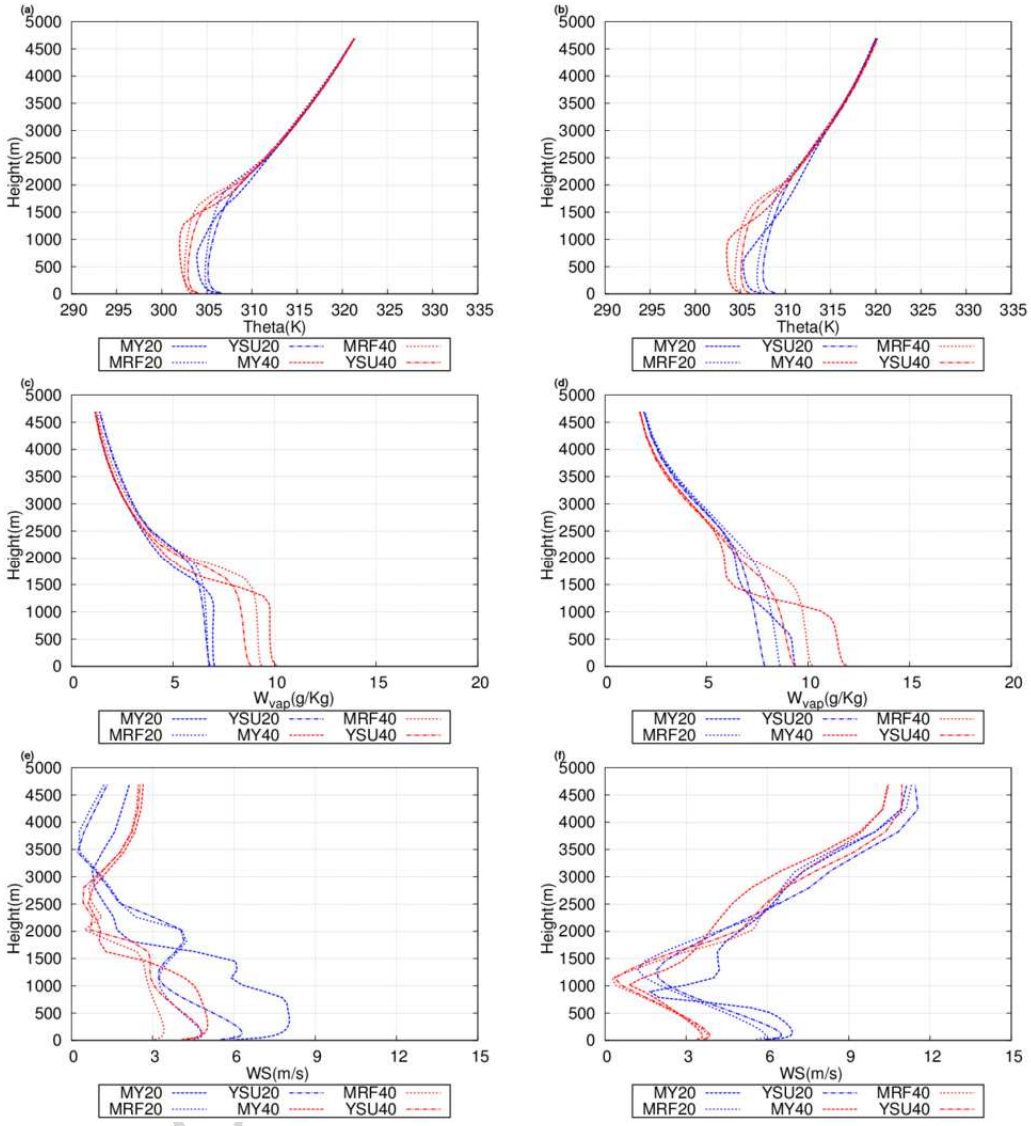

Figure 13

Highlights

The MRF and YSU non-local PBL schemes have been implemented within the RAMS model.

The sensitivity of RAMS to different PBL schemes under mesoscale circulations have been evaluated.

The impact of the initial soil moisture content on these parameterizations has also been evaluated.